DESIGN OF A HEAT EXCHANGER TEST FACILITY

By

Michael Russell Valvo

February, 1998

A Thesis submitted to the
Faculty of the Graduate School of the
State University of New York at Buffalo
in partial fulfillment of the requirements
for the degree of
Master of Science

Acknowledgments

The author would like to thank Dr. William K. George and Dr. James R. Sonnenmeier for their advisement during this project. Thanks are also due to Scott Woodward for his help in the design of the facility. Without their assistance, this work could not have been completed. I would also like to thank my family and Jenn for their constant support. Gratitude is expressed to American Precision Industries for their financial support for this project.

Contents

List of Figures

List of Tables

Abstract

The heat exchanger manufacturing community needs a means to determine the operating conditions and performance of their products. A heat exchanger test facility (HETF) that can be used to generate this information was designed to be capable of testing various sizes of heat exchangers. The HETF is able to operate at a variety of working fluid and air flow rates in which air is used to cool or heat the working fluid. The working fluids are typically water and/or oil. One of the major design issues was diffuser design. Classical design methods were supplemented with a CFD analysis to determine the proper geometry of the diffusers. Measurement devices were selected or designed to measure the air and working fluid flow rates and temperatures. Suitable pumps, blowers, and heating systems were selected to ensure that that HETF will operate under steady conditions. A data acquisition system was developed to allow the user to determine the performance of the heat exchangers and control the components of the HETF.

Chapter 1

Introduction

Heat exchanger manufacturers who wish to remain competitive are continuously engaged in research and development. Heat exchanger test facilities (HETF) are used to evaluate the performance of their ideas and products. These typically consist of a method to induce flow through a heat exchanger, and a means to heat or cool a working fluid and to deliver it to the heat exchanger.

A HETF's main purpose is to determine how the performance of a heat exchanger is related to the operating conditions. The HETF will provide the user with at least the following data: working fluid temperature change, air temperature change, working fluid flow rate, air flow rate, and air pressure drop across the heat exchanger.

1.1 Analyzing HETF Data

Before any analysis can be performed, it is necessary to determine if the data is reliable. If the test section is well insulated, the rate at which heat is gained by the

air is equal to that at which it is lost by the working fluid. Or

$$\dot{Q}_a = \dot{Q}_w \tag{1.1}$$

where $\dot{Q}_a$ and $\dot{Q}_w$ are the respective heat transfer rates. These can be approximately related to the change in temperature of the working fluid through the heat exchanger, ΔT, by

$$\dot{Q} = \dot{m} c_p \Delta T \tag{1.2}$$

where $\dot{m}$ is the mass flow rate and c_p is the specific heat.

Since the flow meters used will be measuring the velocity of the fluids, it will be necessary to convert velocity to mass flow rate by $\dot{m} = \rho A V$. Equation 1.2 becomes

$$\dot{Q} = \rho A V c_p \Delta T \tag{1.3}$$

To determine if the data acquisition system is operating correctly, the user will determine the error between the heat fluxes by

$$error = \frac{\dot{Q}_a - \dot{Q}_w}{\frac{1}{2}\left(\dot{Q}_a + \dot{Q}_w\right)} \tag{1.4}$$

Usually, an error that is within $\pm$ 5% is acceptable. Sources of error include non-uniform velocity and temperature distributions, heat losses through the facility's piping, and instrumentation error. Later chapters will discuss efforts to lessen these sources of error.

Once the data is obtained, it is possible to determine the performance of the heat exchanger. In order to make comparisons between different types of heat exchangers, it is necessary to non-dimensionalize the results. It has been shown [8] that for a counterflow heat exchanger

$$\dot{Q} = U A \Delta T_{lm} \tag{1.5}$$

where U is the overall heat transfer coefficient and ΔT_{lm} is the log mean temperature difference. The latter is defined as

$$\Delta T_{lm} = \frac{\Delta T_2 - \Delta T_1}{ln\left(\Delta T_2 / \Delta T_1\right)} \tag{1.6}$$

where ΔT_1 is the working fluid inlet temperature minus the air outlet temperature and ΔT_2 is the working fluid outlet temperature minus the air inlet temperature. The heat exchangers that will be tested in the facility are typically cross-flow heat exchangers. Equations 1.5 and 1.6 can be used for this type of heat exchanger if a correction factor, F, is introduced which accounts for the difference between counter flow and cross flow heat exchangers. Equation 1.6 then becomes

$$\Delta T_{lm} = F \Delta T_{lm,CF} \tag{1.7}$$

The correction factor is dependent on the temperature differences and is presented graphically in [8]. Since ΔT_{lm} and the heat transfer are known from analyzing the data, equation 1.5 can be solved to find U. Once this is known, it is possible to obtain the average convection coefficient, h. Using this result along with the other data obtained from the HETF, the Colburn j factor (j_H), the Reynolds number (Re), and the friction factor (f) are determined. These are defined as [8]

$$j_H = StPr^{2/3} \tag{1.8}$$

$$Re = \frac{GD_h}{\mu} \tag{1.9}$$

where D_h is the hydraulic diameter and μ is the viscosity. The hydraulic diameter is usually defined as

$$D_h = \frac{4(Area)}{Perimeter}$$

The Stanton number (St=h/Gc_p) and the Reynolds number are based upon the maximum mass velocity, G.

$$G = \rho V_{max} = \frac{\rho V A_{fr}}{A_{ff}} = \frac{\dot{m}}{A_{ff}} = \frac{\dot{m}}{\sigma A_{fr}} \tag{1.10}$$

where A_{ff} is the free-flow area of the finned passages, A_{fr} is the frontal area of the heat exchanger, and σ=A_{ff}/A_{fr}. The friction factor is defined as [8]

$$f = \left[\frac{2\Delta P}{G^2 v_i} - \left(1+\sigma^2\right)\left(\frac{v_o}{v_i} - 1\right)\right]\left[\frac{v_i A_{ff}}{v_m A}\right] \tag{1.11}$$

where v_i and v_o are the fluid inlet and outlet specific volumes and v_m is the average of these values.

Figure 1.1 shows the friction and Colburn factors as a function of the Reynolds number for a heat exchanger tested in the HETF at the Turbulence Research Laboratory (TRL) at the University at Buffalo. The friction factor is the upper curve. Once the non-dimensional performance results are obtained, it is possible to make

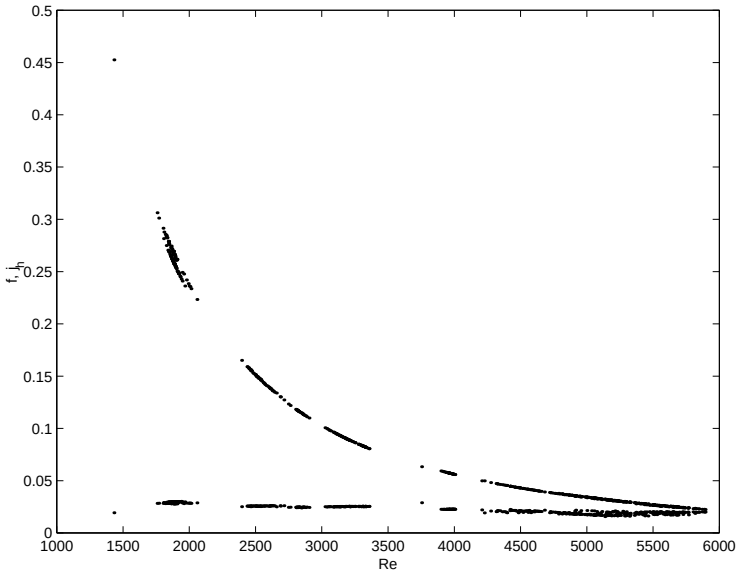

Figure 1.1: Friction and Colburn Factors vs. Reynolds Number

meaningful comparisons between heat exchangers with different configurations.

1.2 An Existing Facility

As a typical example of a HETF, the TRL's facility consists of a wind tunnel that can accommodate various sizes of heat exchangers. A centrifugal blower generates a flow of air which cools the working fluid. The working fluid in this facility is water. An electric boiler can supply up to 70,000 Btu/hr to the working fluid. The water and air flow rates are measured by a turbine meter and pitot tube, respectively. The air and water temperatures are measured with thermocouples.

While the TRL HETF provides useful performance data, it does have some limitations. One of these is the range of operating conditions over which the heat exchangers can be tested. The air flow can only be measured accurately from 1000 to 2800 feet per minute (fpm). This is because the pressure transducers used with the facility do not yield reliable results under 1000 fpm and have an upper limit of 2800 fpm. Another problem is that the tunnel does not have the structural strength to withstand the back pressure imposed by testing cores with high solidity at the higher velocities. Other limitations are that the maximum flow rate of the working fluid is 35 gallons per minute and the facility cannot accommodate other types of working fluids. It is also difficult to change the configuration of the facility to test different sizes of heat exchangers.

1.3 New HETF Specifications

In order to be capable of evaluating their products at a wider range of conditions, the customers have contracted the TRL to design a new HETF with the following specifications:

- The working fluids will be oil and water with flow rates of 10-200 gallons per minute
- The HETF should be able to test cores varying in flow-wise thickness with cross-sectional areas of 1x1 and 2x2 feet
- Down time while the configuration of the tunnel is being changed should be minimal
- The HETF should operate at air speeds up to 4000 fpm
- The HETF should be capable of testing a heat exchanger with a maximum pressure drop across it of 8 in. of water
- The heating system should be able to supply 750,000 Btu/hr while maintaining a constant working fluid inlet temperature
- It should be possible to vary the inlet air temperature
- The data acquisition system should allow the user to control components of the HETF during testing

These specification allow the HETF to be much more versatile than the TRL's facility. It will be easier to test different size heat exchangers at a wider range of operating conditions. The remainder of this report concerns the design procedure, selection of components, and a cost analysis for the new HETF design.

Chapter 2

Design Considerations

The HETF was designed to be capable of testing heat exchangers with cross-sectional areas of 2x2 feet and 1x1 feet. Figures 2.1 and 2.2 are drawings of the facility in each configuration. An isometric drawing of the HETF can be seen in figure 2.3. The largest section of the HETF has a cross-sectional area of 4x4 feet. This occurs between the first expansion (Exp1) and first contraction (Con1) and after the second expansion (Exp22, Exp23). The reason that both expansions expand to this large area will be discussed in chapter 4. The 2x2 test section (Core) is placed after the first contraction which contracts from 4x4 feet to 2x2 feet. After a straight section

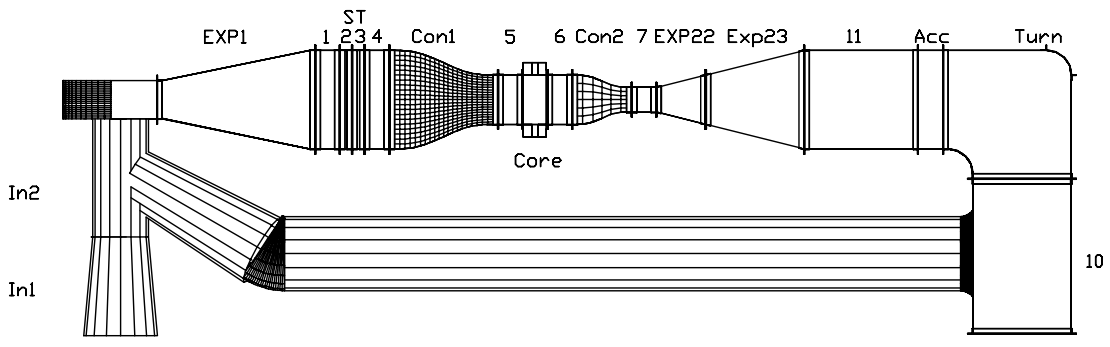

Figure 2.1: Layout for Testing of 2x2 Core

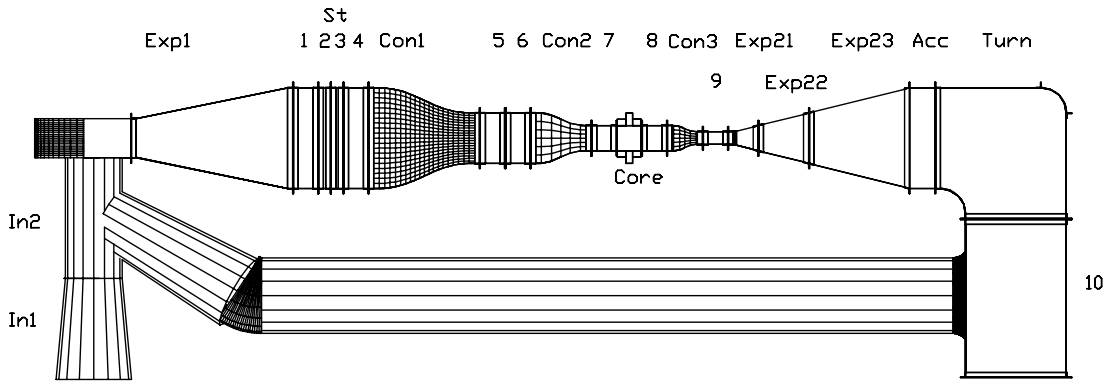

Figure 2.2: Layout for Testing of 1x1 Core

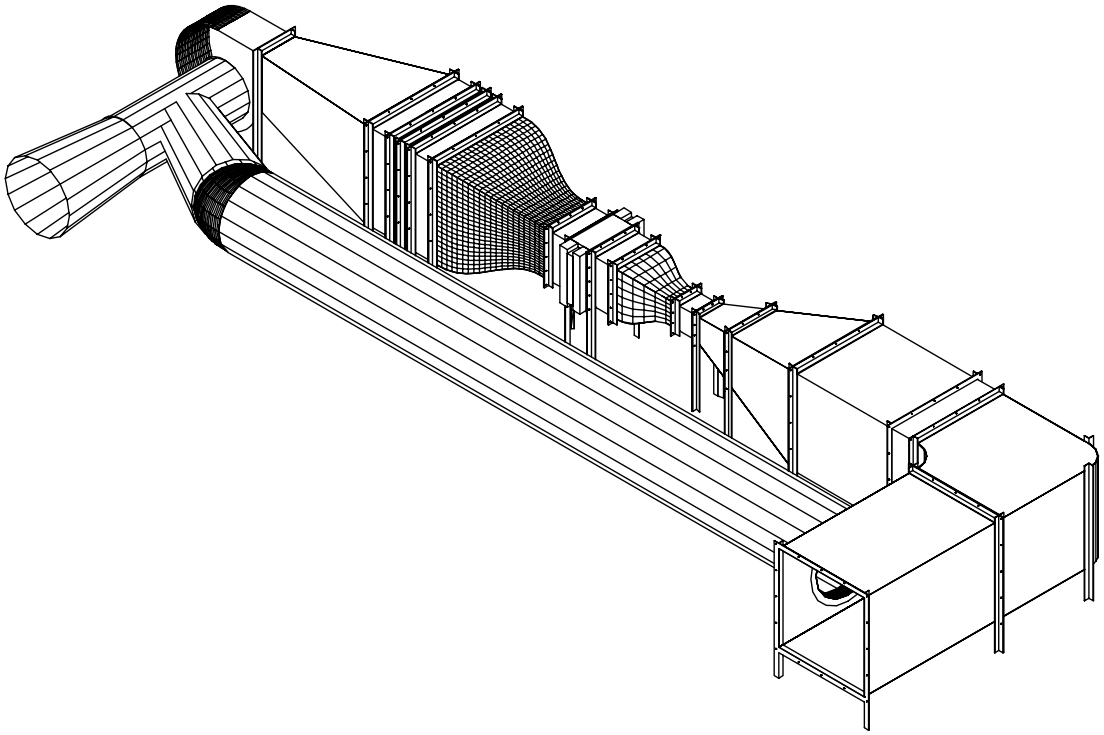

Figure 2.3: Isometric Drawing of 2x2 Configuration

(6), another contraction (Con2) brings the area down to 1x1 feet. The reason for this contraction will be discussed in chapter 5. After another straight section (7), the second expansion expands the facility to 4x4 feet. The expansion is followed by a long straight section (11), an adjustable section (Acc), a turning section (Turn), and finally another long straight section (10) which leads to the outlet. Return ducting attached to the last straight section allows some of the heated air to be returned to the inlet. When a 1x1 heat exchanger is being tested, the straight section after the second expansion is removed. The second expansion is then attached to the adjustable section. The test section is placed after the second contraction. A third contraction (Con3) which contracts down to an area of 0.5x0.5 feet is located after the test section. The facility then expands to the 4x4 area. It was decided that the majority of the HETF will be constructed out of 18 gauge sheet metal. This was selected because of its ease of manufacturing, cost, and weight. Flanges to connect the sections are made out of 0.25" thick angle iron.

As it can be seen in figure 2.3, some of the flanges have legs attached to them which support the facility. These legs will have wheels attached to them which allow individual components to be removed and shifted easily when changing testing configurations. An angle iron track will guide these wheels.

2.1 Plumbing

One of the major goals with the design of the HETF is versatility. Heat exchangers with varying thicknesses and different types of inlet and outlet configurations are to be tested with the facility. As a result of this, the exact location of the test section in the tunnel will vary. The majority of the system's plumbing is made from flexible

hose to accommodate this. Therefore, the user will not need to be concerned with the exact placement of the core during installation for a test as the plumbing will accommodate various positions.

To allow ease of operation, it was decided to have two separate piping systems for the different working fluids. This will allow a quicker change-over because the user will not have to clean the entire piping system when the working fluid is changed. In the long run, the reduced operating costs will offset the increased capital cost associated with the two systems.

2.2 Inlet Air Temperature Variation

In order to test the heat exchangers at a variety of conditions, it is necessary to vary the inlet air temperature by heating or cooling the air. To heat the inlet air, ducting has been designed that mixes heated air exiting the facility with the inlet air. A damper on the ducting controls the amount of heated air that is vented back to the system.

One method to cool the inlet air was to add a cooling system. This would include a heat exchanger that would be placed in the facility to cool the air before the test section. It was decided that the increased cost with this option was undesirable. Therefore, the facility was designed to have the ability to use outside air for testing. This would give a wide variety of inlet air temperatures for testing depending on the time of the year.

2.3 Expansions

The design of the diffusers is one of the most critical aspects of the HETF design. One of the largest sources of pressure loss in the facility is the diffusers. This is because a typical feature of diffusers is strong adverse pressure gradients. It has been shown that boundary layers grow in thickness and eventually separate in adverse pressure gradients [17]. This separation is called stall and causes a dramatic decrease in diffuser performance. Kline [12] and Kline et al [11] present results concluding that diffuser performance is related to the divergence angle, 2θ, and the centerline length to width ratio, N/W. Certain combinations of these factors will cause stall to occur in the diffuser.

With respect to stall, fluid flow is categorized into four classes [16]. Figure 2.4 illustrates where these flow regions lie with respect to N/W and 2θ. The first region is below line a-a in the figure and is categorized as unstalled flow. In this region, the boundary layers sometimes become thick but there is very little stall. The flow is uniform and constant in time. The next region, between a-a and b-b, is large transitory stall. Flow in this region fluctuates with time. Stalled regions form and are swept out of the diffuser. The third region is two-dimensional stall and lies above line b-b. This stall is mostly steady, although there are some unsteady areas around the mixing region. The stalled regions block the inlet area, which causes a decrease in diffuser performance. The last region is jet flow. This region begins anywhere between lines d-d and c-c. The region between these lines is the hysteresis region. In this regime, jet flow and two-dimensional flow can occur. Jet flow is also steady. The flow separates on the walls close to the inlet and continues down the diffuser. Figure 2.5 illustrates the different classes of stall. The static pressure recovery coefficient, C_p, is one factor which is used to determine diffuser performance. Its dependence on

the divergence angle is illustrated in figure 2.6. An expansion with the necessary

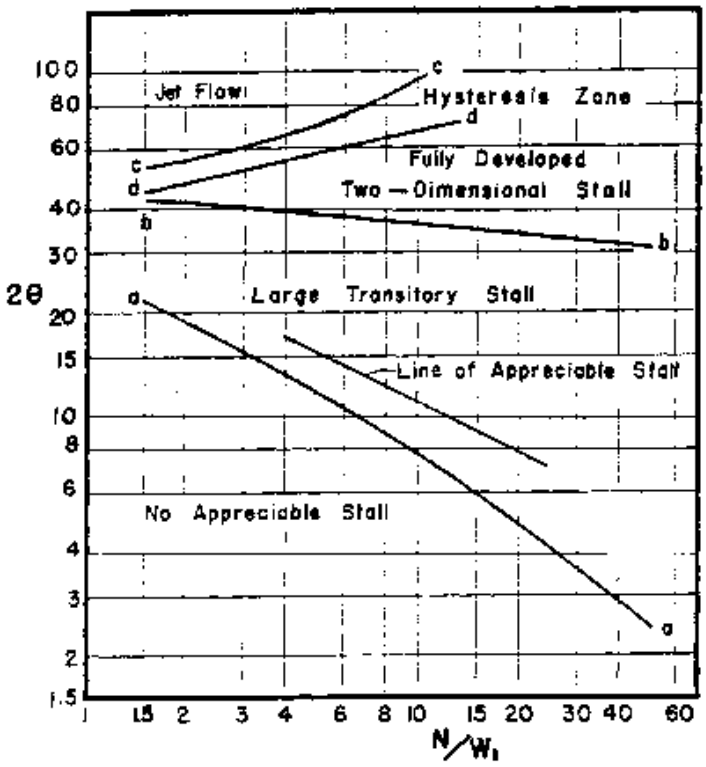

Figure 2.4: Regimes of flow for two dimensional plane-walled diffusers [16]

dimensions for the HETF would have a divergence angle of 23° and N/W of 4. As it can be seen in figure 2.4, this falls into the region of transitory stall. One way to ensure that the diffuser geometry does not promote stall is to use splitter plates in the diffuser. When this is done, it should be remembered that stall is dependent on 2θ *and* N/W. For example, a diffuser with N/W=10 and 2θ=30 lies in the transitory stall region. If two splitter plates section the diffuser along the entire length into three sections with 2θ=10, N/W becomes 30. This would still cause the flow to lie in the transitory regime. Kline [12] has found that this can be averted by using splitters that do not run down the entire length of the diffuser. This decreases 2θ the same

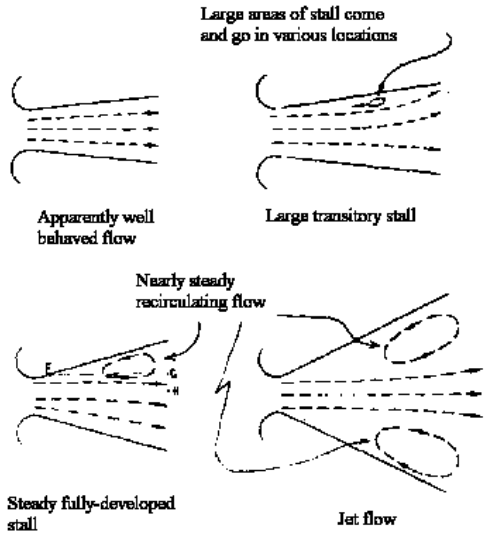

Figure 2.5: Schematic diagrams of regimes of diffuser flow [12]

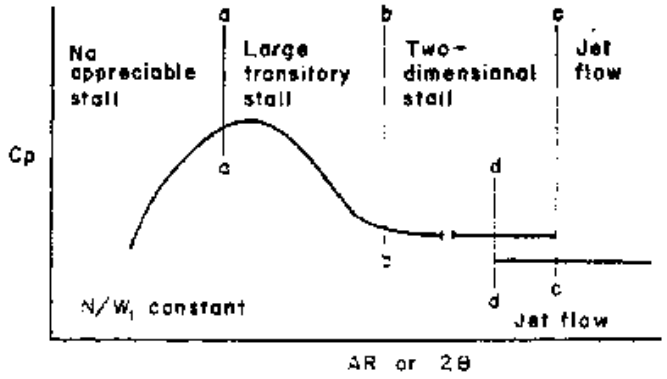

Figure 2.6: Relationship between flow regimes and a pressure recovery curve [16]

amount but does not increase N/W as much. This will allow the flow to be in the unstalled regime. It was determined that for the diffuser in this case, splitters that run the entire length could be used. This creates 12 individual cells with divergence angles of 5.5° and N/W=12. Figure 2.4 shows that this flow will be in the unstalled region.

Since the inlet to the second expansion will vary in cross section depending on the size of heat exchanger being tested, the expansion is separated into 3 sections. When a 2x2 heat exchanger is being tested, the first section will be removed. The dimensions of the second expansion are similar to the first expansion. Therefore, it also uses splitters which create 16 cells with divergence angles of 7°. The diffuser angles for both expansions will ensure that the diffusers will behave as expected. Figures 2.7 and 2.8 show the two expansions. Further details about the performance of the diffusers are given in chapter 4.

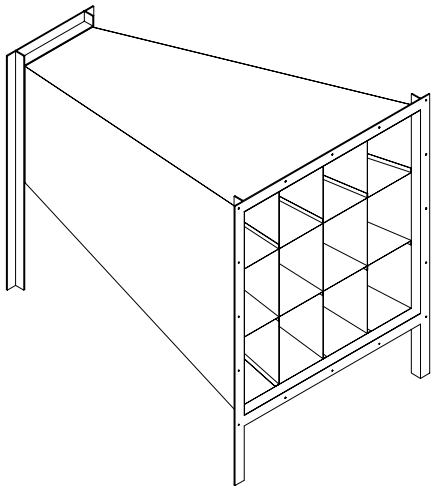

Figure 2.7: Drawing of Expansion 1

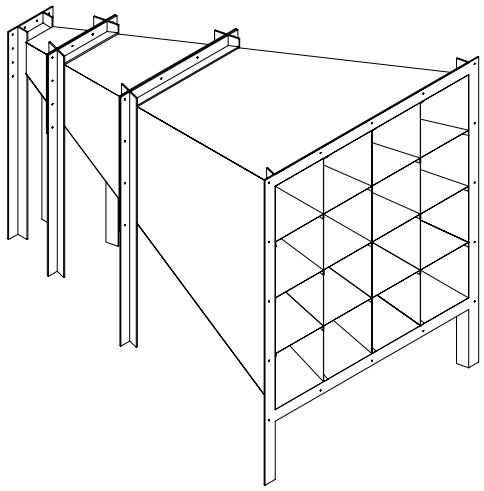

Figure 2.8: Drawing of Expansion 2

2.4 Straight Sections

Most of the straight sections, figure 2.9, are made from sheet metal and have square cross sections. To make the test section visible to the user, the straight sections after the test sections have clear lexan sides. This allows for easier installation of instrumentation. Flow conditioning takes place in the third straight section. The flow conditioning includes two screens to reduce turbulence and a section of straws to straighten the flow. This makes the flow uniform which allows for more accurate and reliable results. If the flow was not uniform, it would be difficult to obtain the average velocity which is used in the performance calculations.

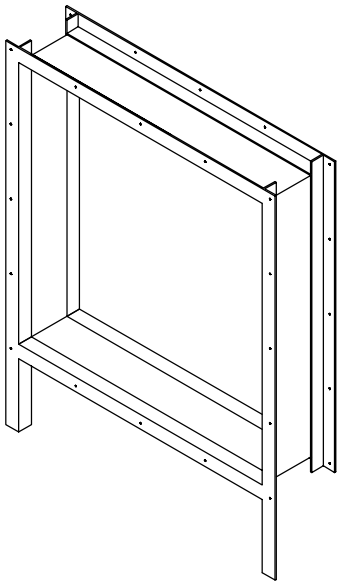

Figure 2.9: Drawing of a Straight Section

2.5 Contractions

The purpose of a contraction, figure 2.10, is to increase the velocity of the fluid while maintaining a uniform flow. The uniformity of the flow is dependent on the contraction ratio, length of the contraction, and the contour of the contraction. Two popular methods that are used to determine the contour of a contraction are the matched cubic technique and the fifth order polynomial technique. The matched cubic technique uses two cubic equations[3]. The first equation determines the contour from the inlet of the contraction to the matching point. The second equation evaluates the contraction's contour after the matching point to the outlet of the contraction. These equations are

$$y_1 = a + bx + cx^2 + dx^3$$

$$y_2 = e + fx + gx^2 + hx^3$$

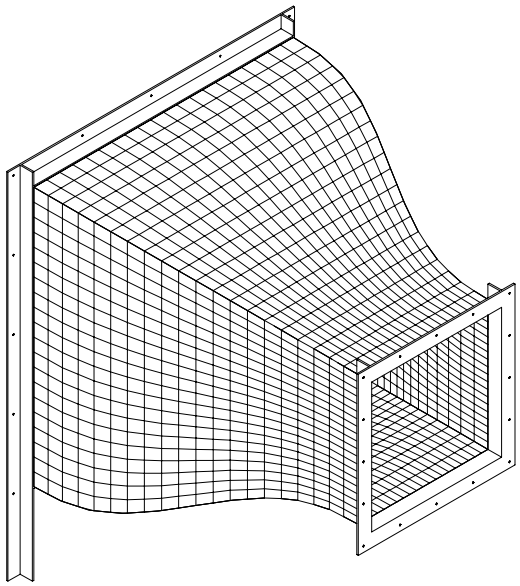

Figure 2.10: Drawing of a Contraction

To determine the coefficients of these equations, eight boundary conditions are needed. The first six conditions are evaluated at the inlet and outlet of the contraction. At these points, the positions are known and the first and second derivatives of the equations are set to zero. The final two boundary conditions are evaluated at the matching point. At this point the position and slope must be the same for each equation. These conditions are shown below. The inlet half width is h_1, h_2 is the outlet half width, and x_m is the point at where the two equations are matched. With

x=0	x=L	$x=x_m$
$y_1 = h_1$	$y_2 = h_2$	$y_1 = y_2$
$\frac{dy_1}{dx} = 0$	$\frac{dy_2}{dx} = 0$	$\frac{dy_1}{dx} = \frac{dy_2}{dx}$
$\frac{d^2y_1}{dx^2} = 0$	$\frac{d^2y_2}{dx^2} = 0$	

these boundary conditions, the preceding equations are solved to obtain:

$$y = (h_1 - h_2)\left[1 - \frac{1}{X^2}\left(\frac{x}{L}\right)^3\right] + h_2,\ x < x_m$$
$$y = \frac{(h_1 - h_2)}{(1-X)^2}\left(1 - \frac{x}{L}\right)^3 + h_2,\ x > x_m$$

where X=x_m/L.

The alternate method uses a fifth order polynomial given as:

$$y = a + bx + cx^2 + dx^3 + ex^4 + fx^5$$

Six boundary conditions are needed to determine the coefficients for this equation. These boundary conditions are the same as the conditions imposed at the inlet and oulet for the matched cubic technique. Using these boundary conditions, the fifth order polynomial is found to be

$$y = h_1 - 2\,(h_1 - h_2)\,[5\chi^3 - 7.5\chi^4 + 3\chi^5]$$

where χ=x/L. Figure 2.11 shows the contours generated by the two techniques.

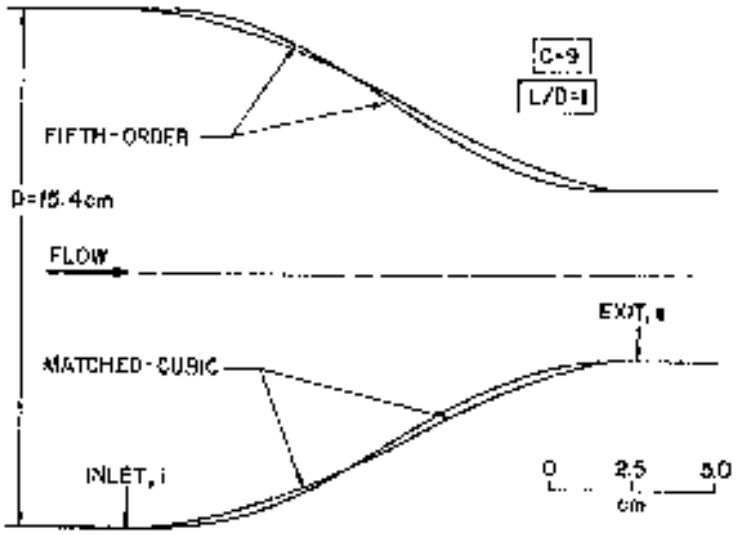

Figure 2.11: Matched Cubic and Fifth Order Polynomial Curves [19]

While the matched cubic technique is more popular than the fifth order, there is a problem associated with it. It has been shown that the flow is non-uniform at the outlet. The flow at the edges is slightly faster than at the center. Tan-Atichat[19] determined that this non-uniformity is much less for the fifth order contour than for the matched cubic contour. This is illustrated in figure 2.12. George [4] has suggested that this is due to the fact that the matched cubic profile has a discontinuity in curvature at the matching point, whereas the fifth order polynomial has no such discontinuity. Since it is desired to have a flow as uniform as possible, it was decided to use the fifth order polynomial contour for the contractions.

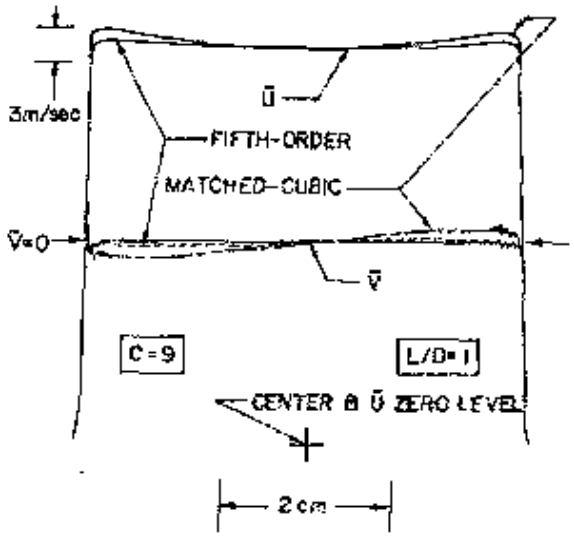

Figure 2.12: Nomalized lateral profiles of mean and turbulence velocities downstream of matched cubic and fifth order contractions
[19]

The length to inlet diameter (L/D) ratio also has an effect on the non-uniformity at the exit. Figure 2.13 shows the mean velocity distribution for a L/D of 0.5,1.0, and 1.5. It is evident that the velocity variation decreases for larger L/D values. In order to minimize the length of the HETF, it was decided to use a L/D of 1.0.

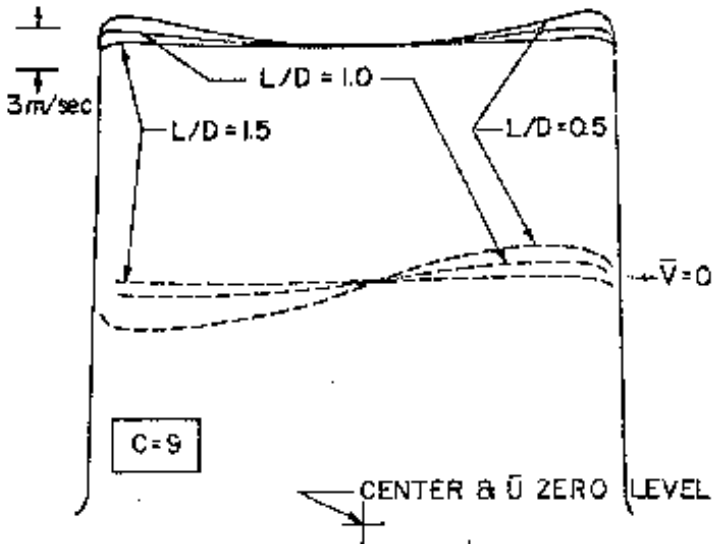

Figure 2.13: Normalized lateral profiles of mean and turbulence velocities downstream of contractions with different L/D ratio
[19]

2.6 Adjustable Section

Since the facility will be testing heat exchangers varying in thickness, the HETF was designed to have its length adjustable. This was accomplished by designing an adjustable section, figure 2.14. This is composed of two sections with one having a smaller cross sectional area than the other, allowing the smaller section to slide inside the larger section. This section is 10 inches long when compressed and 16 inches long when expanded. This gives 6 inches of freedom which will make the thickness of the test sections less critical. The section will be sealed on the outside to prevent air leakage. The adjustable section has a 4x4 cross section so that there is no appreciable change in area.

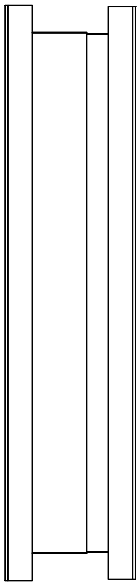

Figure 2.14: Drawing of Adjustable Section

2.7 Turning Section

The layout of the building where the HETF will be operated in requires that the inlet and the outlet of the facility must be on the same wall. Therefore, it was necessary to design a turning section, figure 2.15. It is common practice to incorporate turning vanes into a turning section. It is possible for a flow to lose all of its pressure in a corner if there are no turning vanes [10]. To lessen the pressure drop through the corner, four turning vanes are used in this section.

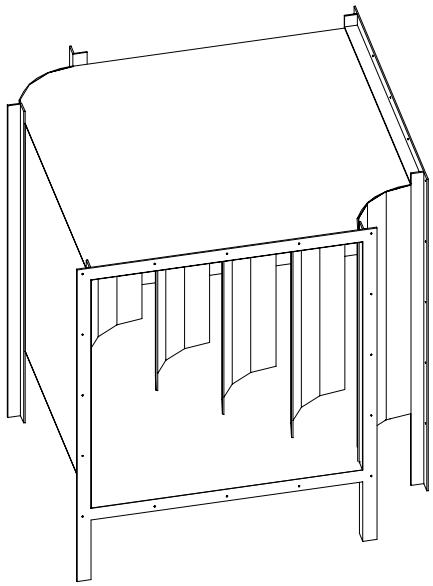

Figure 2.15: Drawing of the Turning Section

Chapter 3

Boiler and Pump Selection

The pumps and boiler were selected so that they fulfill all of the design criteria. An electric boiler was decided upon because it will be less expensive to operate than a natural gas boiler at the customer's facility.

3.1 Boiler

In order to obtain consistent and valid results when using the HETF, it is important to test the heat exchangers at a steady state. The variables in the HETF that the user can control are air flow, working fluid flow, air inlet temperature, and working fluid inlet temperature. If the pumps and blower are operating correctly, the flow rates will be constant. Since the heated air exits into the room which houses the HETF, the inlet air temperature will increase during a day of testing. During one test, this variation is small enough that it doesn't affect the validity of the test. However, the user should keep the changing temperature in mind when calculating the properties of air. Therefore, the only unsteady factor that causes concern is the inlet working fluid temperature.

3.1.1 Temperature Control

Control systems that are used in temperature control are closed-looped feedback systems. The controller determines the error, e(t), between the actual temperature of the working fluid, T_a, and the desired temperature, T_s. Or, e(t)=$T_s - T_a$. An output signal, m(t), is then generated which will reduce the error. Common systems are on-off, proportional, integral, proportional plus integral (PI), proportional plus derivative (PD), and proportional plus integral plus derivative (PID) [14].

On-off Controllers

The simplest control system is an on-off system. The boiler will heat up to T_s and then shut off. When the temperature falls below T_s, the boiler will turn on again. The output signal is given by:

$$m(t) = M_1, \text{ for } e(t) > 0$$
$$m(t) = M_2, \text{ for } e(t) < 0$$

For temperature control, M_2 is zero. When T_a is greater than T_s, no heat will be supplied to the working fluid. The problem with this type of control is that a steady state will never be reached. The system reacts only when the temperature departs from T_s. This causes the temperature to oscillate around the set point, figure 3.1. The boiler in the TRL's HETF uses this type of control. Figure 3.2 shows the working fluid inlet and outlet temperature variation during a previous heat exchanger test performed with the HETF. The inlet temperature is the upper curve. The inlet temperature varies from 185°F to 189°F. As a result of this oscillation, both the temperatures and the temperature difference are varying. This makes it very difficult to obtain reliable results.

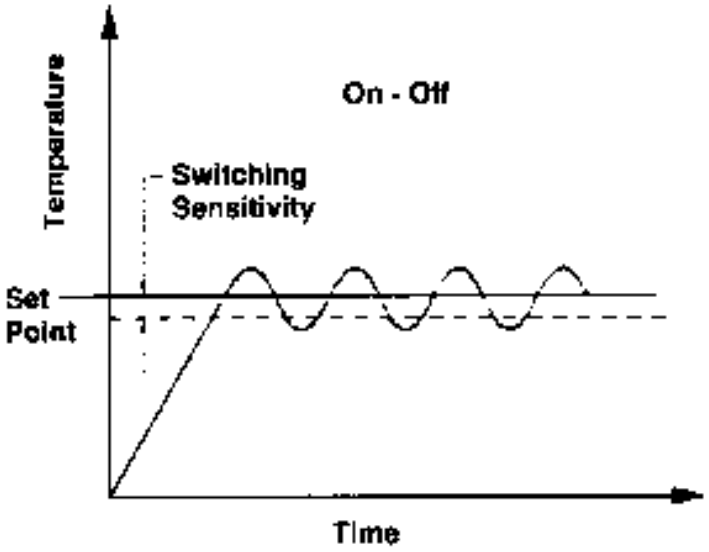

Figure 3.1: On-Off Control

[20]

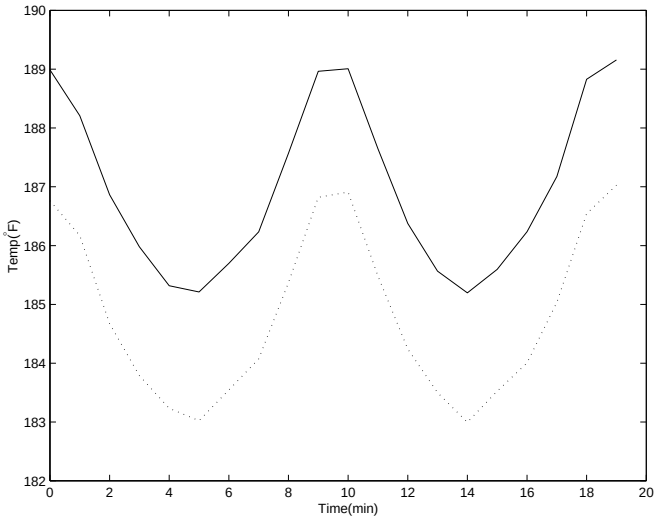

Figure 3.2: Temperature vs. Time

Proportional Controllers

A proportional controller's output signal is dependent on the magnitude of the error.

$$m(t) = K_p e(t)$$

where K_p is the proportional sensitivity, or gain. This allows the heat input to be scaled back as the error approaches zero, which reduces the overshoot that is present with the on-off control. For temperature control, the control is on until the temperature reaches the proportional band. Then the proportional control begins to lessen the heat input. This is done by turning the heat input on and off. The ratio of on time to off time determines how much heat is being put into the system. The problem with a proportional control is the steady state temperature. In order for the system to be at steady state, the boiler needs to supply the same amount of heat that is being rejected by the heat exchanger. When the temperature of the fluid approaches T_s, the error approaches zero. This causes m(t) to become zero and therefore no heat is being added to the system even though heat is being rejected. As a result of this, the temperature would oscillate similar to the on-off control. To prevent this from happening, the working fluid temperature is stabilized at a temperature below T_s. Therefore, there will always be an error so heat can be added to the system. This offset, or droop, can be reduced by increasing the gain. Too large a gain will cause the system to oscillate. This offset can be eliminated without causing oscillations by adding an integral function [14]. Figure 3.3 illustrates a proportional control.

Integral Control

An integral control has an output signal that varies at a rate proportional to the error signal.

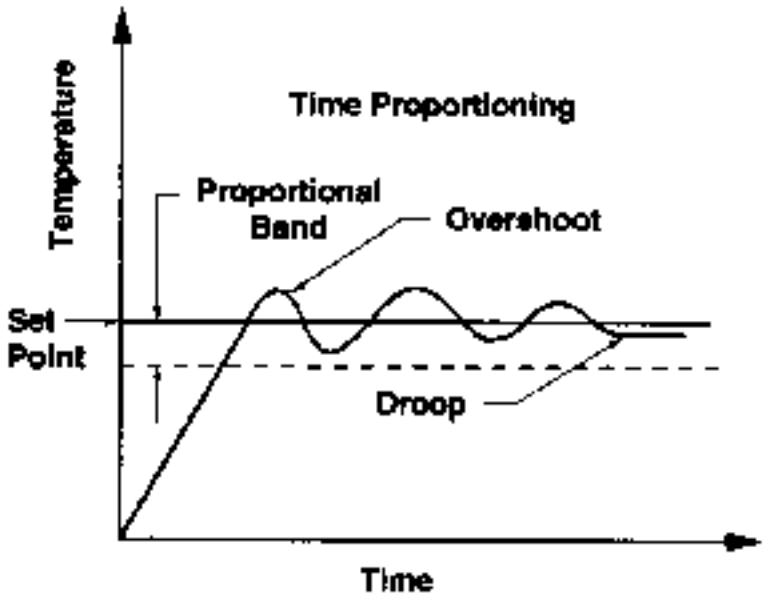

Figure 3.3: Proportional Control

[20]

$$\frac{dm(t)}{dt} = K_i e\,(t)$$

Or

$$m\,(t) = K_i \int_0^t e\,(t)\,dt$$

For an integral control, m(t) at any time is the area under the error curve up to that point. Therefore, m(t) can be nonzero even when e(t) is zero. This control method does not have the offset error that the proportional method has.

Proportional Plus Integral Control

An integral control is usually combined with a proportional control. The output signal for a PI control is given by

$$m\,(t) = K_p e\,(t) + \frac{K_p}{T_i} \int_0^t e\,(t)\,dt$$

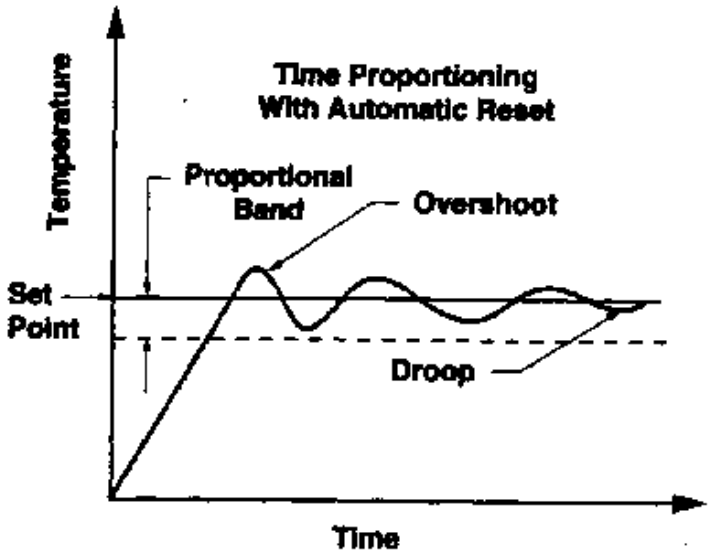

Figure 3.4: PI Control

[20]

where T_i is the integral time. The integral portion of the control is an automatic reset which shifts the proportional band upwards to compensate for an offset before it exists [20]. Figure 3.4 shows the behavior of a PI control. This type of control combines the benefits of proportional and integral controls and therefore it eliminates the offset error.

Proportional Plus Derivative Control

A PD control's output signal is

$$m(t) = K_p e(t) + K_p T_d \frac{de(t)}{dt}$$

where T_d is the derivative time. This type of control has an output which is dependent on the rate of change of the error. If the error is changing at a fast rate, the PD control responds with a correction before the error will get too large. This control is anticipatory and thereby reduces overshoot. This is especially useful when there is a

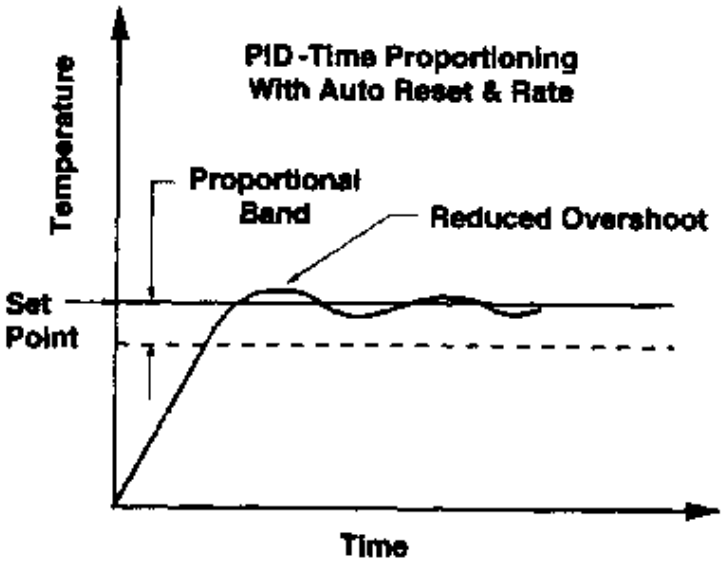

Figure 3.5: PID Control

[20]

disturbance in the system, such as a change in the heat being rejected by the heat exchanger. The derivative control can not be used by itself because it only operates when the error is changing.

Proportional Plus Integral Plus Derivative Control

The PID control has an output signal given by

$$m(t) = K_p e(t) + \frac{K_p}{T_i} \int_0^t e(t)\, dt + K_p T_d \frac{de(t)}{dt}$$

This type of control reaches the setpoint quickly with a smaller overshoot, has no offset, and does not have an oscillation. The PID control is illustrated in figure 3.5. This control is useful when a steady temperature is needed in a system that is exposed to disturbances, which are characteristics of the HETF. The disadvantage of a PID control is the cost, which is more than a simple control.

Another factor that influences the inlet temperature is the heat load. In order for the inlet temperature to be constant, the boiler must supply the same amount of heat that is being rejected by the heat exchanger. It was decided that a boiler that can supply 750,000 BTU/hr will supply enough heat to maintain steady state for all heat exchangers to be tested with the facility.

3.2 Pumps

Three pumps are used in the facility. The first is a circulator pump which delivers heated water from the boiler to a shell and tube heat exchanger where the heat is transfered to the working fluid. The other pumps are used to deliver the heated working fluid to the heat exchanger being tested. Two pumps are required because of the two different working fluids.

The customer had stipulated that the working fluid should be supplied at a pressure of 25psi. This will be enough pressure to overcome losses in the piping and all of the heat exchangers that will be tested. Pumps were selected that can supply this pressure at the entire range of flow rates.

Chapter 4

Blower Selection

When designing the HETF, one of the objectives was to minimize the pressure drop through the facility. This will allow for a smaller and less expensive blower to be used. Despite efforts in this regard, it is unavoidable that there will be a significant pressure loss through the facility. The sources of the pressure loss will be discussed in the following section.

4.1 Calculation of Coefficient of Pressure Loss

There is a loss of energy through each section of the HETF as a result of friction and geometry. This loss of energy is expressed as a total pressure loss. The coefficient of total pressure loss, K_t, is defined as[5]:

$$K_t = \frac{\Delta P_t}{\frac{1}{2}\ \rho U^2} \tag{4.1}$$

where U is the average inlet velocity and ΔP_t is the total pressure loss. This coefficient is found experimentally and analytically depending on the geometry of the component. Some simple cases, such as a sudden opening, have a purely analytical

solution. In order to determine the pressure loss through the facility, it was necessary to estimate the losses through each section. A combination of both techniques is used to find the losses in a straight section. Experimental results are used to determine K_t for expansions, contractions, turning sections, and flow conditioning [18]. The next sections discuss how the pressure loss for each section of the tunnel was determined.

4.1.1 Straight Sections

The pressure loss in a straight duct is a function of the Reynolds number, the length of the section, and the surface roughness of the section [18]. Using dimensional analysis it can be shown that

$$\frac{\Delta P}{\frac{1}{2}\rho U^2} = G\left(\frac{\rho U D}{\mu}, \frac{L}{D}, \frac{e}{D}\right) \tag{4.2}$$

where ρ is the density of air, D is the diameter of the section, μ is the viscosity of air, L is the length of the section, and e is the surface roughness of the section. This gives a finite number of parameters to determine the pressure loss. It should be evident that the pressure drop increases as the length of the section increases, or $\Delta P \propto L$. Therefore

$$\frac{\Delta P}{\frac{1}{2}\rho U^2} = \frac{L}{D}\lambda\left(\frac{\rho U D}{\mu}, \frac{e}{D}\right) \tag{4.3}$$

where λ, the skin friction coefficient, is some unknown function dependent on the Reynolds number and the surface roughness. Finally,

$$K_t = \lambda\frac{L}{D} \tag{4.4}$$

The skin friction coefficient is found by utilizing experimental results. It was determined by using correlations presented in [5] that λ remained constant to within 2% at 0.01 for the range of velocities that will be used in testing.

4.1.2 Expansions

The first expansion was sectioned into twelve equal rectangular expansions, as described in chapter 2. Figure 4.1 shows the expansion with one of these sections next to it. The inlet area of each section is $0.29ft^2$ and the exit area is $1.33ft^2$. The divergence angle, 2θ, is 5.5°. Losses occur in these expansions as a result of wall friction and the expansion. There are two methods available to determine the coefficient of pressure loss. The first method uses an empirical relation given by Pope and Rae[10].

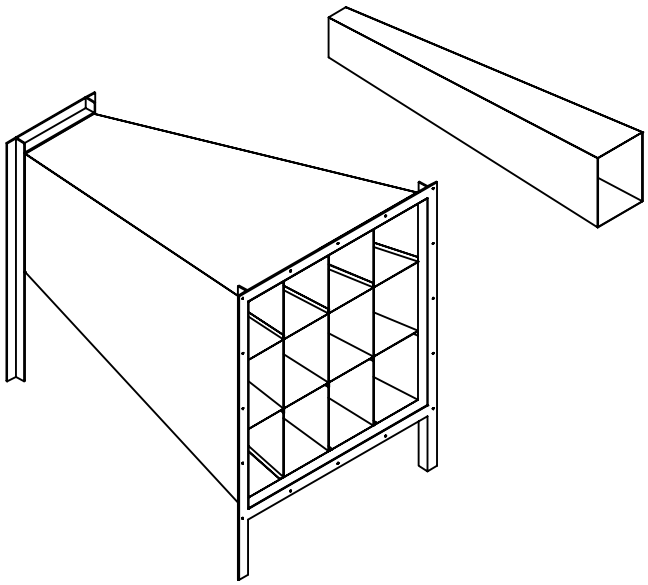

Figure 4.1: Drawing of Expansion 1

$$K_t = \left(\frac{\lambda}{8\tan\theta} + 0.6\tan\theta\right)\left(1 - \frac{A_{in}^2}{A_{out}^2}\right) \tag{4.5}$$

Using this relation, K_t was found to be 0.053.

Kline et al[11] and Runstadler et al[9] use a collection of diffuser data to predict the performance of diffusers. They introduce two other parameters used to determine diffuser performance. These are the coefficient of pressure recovery, C_{pr}, and the

pressure effectiveness, η_p. These are defined as[11]

$$C_{pr} = \left[\frac{1}{Ao}\int_{A_o} P_o dA_o - \frac{1}{Ai}\int_{A_i} P_i dA_i\right]\left[\frac{1}{A_i}\int_{A_i}\frac{1}{2}\rho U_i^2 dA_i\right]^{-1} \tag{4.6}$$

$$\eta_p = \frac{C_{pr}}{C_{pri}} \tag{4.7}$$

where C_{pri} is the ideal pressure recovery coefficient. For one dimensional flow, equation 4.6 becomes

$$C_{pr} = \frac{(P_o - P_i)}{\frac{1}{2}\rho U_i^2} \tag{4.8}$$

where P_o and P_i are the outlet and inlet static pressure. Using Bernoulli's equation, 4.9, along with the continuity equation, it is possible to determine C_{pri}.

$$P_o + \frac{1}{2}\rho U_o^2 + \Delta P_{total} = P_i + \frac{1}{2}\rho U_i^2 \tag{4.9}$$

For an ideal case, $\Delta P_{total} = 0$. Equation 4.9 becomes

$$P_o - P_i = \tfrac{1}{2}\rho U_i^2\left(1 - \tfrac{1}{AR^2}\right)$$

$$C_{pri} = 1 - \frac{1}{AR^2} \tag{4.10}$$

where AR is the area ratio.

The three diffuser performance parameters, K_t, C_{pr}, and η_p, have optimum values at different values of 2θ. Since this discussion is interested in the total pressure loss, it is required to convert C_{pr} from Kline's data to K_t. This is done by using equation 4.9 again.

$$P_o - P_i + \Delta P_{total} = \tfrac{1}{2}\rho U^2\left(1 - \tfrac{1}{AR^2}\right)$$

$$\tfrac{P_o - P_i}{\frac{1}{2}\rho U_i^2 C_{pri}} + \tfrac{\Delta P_{total}}{\frac{1}{2}\rho U_i^2 C_{pri}} = 1$$

$$\tfrac{C_{pr}}{C_{pri}} + \tfrac{K_t}{C_{pri}} = 1$$

$$K_t = C_{pri} - C_{pr} \tag{4.11}$$

It was found by using figure 4.2 and equation 4.11 that K_t is about 0.07. This value is close to what was found by using equation 4.5. The former value will be used for two reasons. The first is that no graphical interpolation is required. It also includes the skin friction coefficient which takes into account the velocity of the fluid and the material properties of the section.

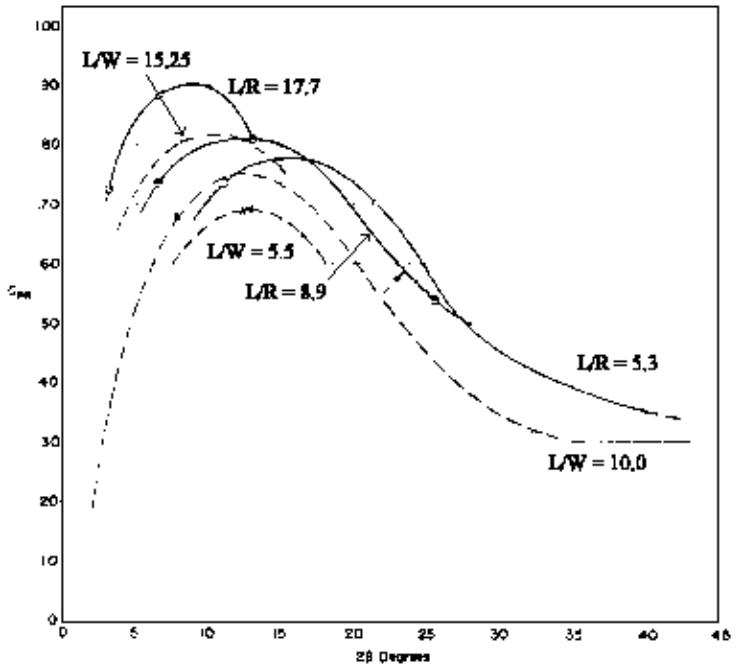

Figure 4.2: Two dimensional diffuser performance [11]

It will be shown in section 4.1.3 that the pressure loss coefficient through the flow conditioning is very large. Equation 4.1 shows that $\Delta P \propto \frac{1}{2}\rho U^2$. Therefore, to lessen the pressure drop through the flow conditioning it is necessary to lower the velocity of the air. The expansion decreases the velocity by 4 times for the 2x2 cores and by 16 times for the 1x1 cores. This reduces the pressure loss through the conditioning by 16 times for the large cores and by 256 times for the small cores. These losses are determined in section 4.2.

The pressure drop caused by the second expansion was found by using equation 4.5. The expansion was sectioned into 16 equal rectangular expansions. The dimensions of the cells for the first section of the second expansion are: $A_{in} = 0.016ft^2, A_{out} = 0.0625ft^2, 2\theta = 7°$. It was then found that $K_t = 0.054$. Since the geometric factors are the same for each of the three sections of the second expansion, K_t will also be the same for each section.

The purpose of the second expansion is to recover the static pressure. If the HETF was not expanded to the larger area, the exit velocity would approach 16,000 fpm. This would lead to a pressure loss of about 16 inches of water. The expansion slows down the air which causes a much less pressure loss. It is also not desired to have a jet exiting the facility at such a high velocity.

A CFD study concerning the effects of divergence angle on diffuser performance with respect to pressure recovery was performed. This was done to complement the techniques used in this chapter. It was found that the CFD results confirmed the results presented by Kline [11] for the smaller divergence angles. The CFD results were invalid for angles above 15°. The reasons for this, along with the study's results, can be found in appendix A.

4.1.3 Flow Conditioning

The flow conditioning that will be used in this tunnel will consist of a layer of straws between two screens. The pressure losses associated with the flow conditioning is found based upon experimental evidence.

Straws

Pope and Rae [10] state that for a honeycomb arranged in a similar manner to this design, K_t is 0.3. This value is for a length to diameter ratio of the straws, L/d, of 6. For the present case, L/d is 24. Therefore K_t will be assumed to be 1.2.

Screens

The pressure loss coefficient for damping screens is given by [10]

$$K_t = K_o + \frac{55.2}{R_d} \tag{4.12}$$

where

$$K_o = \left(\frac{1-0.95\beta}{0.95\beta}\right)^2$$

and

$$\beta = \frac{Projected\ open\ area}{Total\ Area} = \left(1 - \frac{d}{M}\right)^2$$

$$d = wire\ diameter$$

$$M = mesh\ length$$

R_d = Reynolds number based on wire diameter, d

It was found that for the higher velocities, the pressure loss through the flow conditioning is 0.43 inches of water, or 25% of the loss through the facility. This loss is unavoidable since a well conditioned flow is necessary for proper testing.

4.1.4 Contractions

The losses in the three contractions are a result of friction. K_t for the contractions can be found by the following expression [5].

$$K_t = \frac{4}{9}\ \lambda \frac{L}{D_h}\ \frac{n^{\frac{9}{2}} - 1}{n^{\frac{5}{2}}\ (n-1)} \tag{4.13}$$

$$K_t = 0.0237$$

where

$$\frac{L}{D_h} = 1$$
$$n = \frac{A_{in}}{A_{out}} = 4$$

These geometric factors are the same for all three contractions. Therefore K_t will also be the same. K_t for the contraction before the fan was found in the same manner.

4.1.5 Losses Through the Heat Exchangers

The losses associated with the heat exchangers were evaluated under three conditions provided by the manufacturer: best case with no pressure loss across the heat exchanger, worst case with $\Delta P = 8$in, and ΔP evaluated from previous data.

Best Case

For the best case, ΔP is 0. Therefore from equation 4.1 $K_t = 0$. This will give the pressure drop across the HETF with no heat exchanger present.

Worst Case

The worst case is evaluated using a ΔP across the heat exchanger of 8in of water. Using equation 4.1 is was possible to determine K_t for each core at a variety of

velocities. This determined what the maximum pressure drop through the HETF is.

Table 4.1: K_t for Worst Case for 2x2 Core

Velocity(fpm)	Dynamic Pressure (in. water)	K_t
1000	0.063	127.80
2000	0.250	31.95
3000	0.563	14.20
4000	1.002	7.99

Previous Data

Heat exchangers similar to the ones for which the HETF is designed for have been tested previously in the TRL. Using equation 4.1 and data collected from these heat exchangers, it was possible to determine K_t for a typical core. The results from these tests are given in table 4.2. This case shows how the HETF will perform under typical operating conditions.

Table 4.2: K_t for Previous Data

Velocity(fpm)	ΔP (in. water)	K_t
1000	0.03	0.479
2000	0.10	0.400
3000	0.21	0.373
4000	0.45	0.449

4.1.6 Turning Section

The pressure loss in the turning section is a result of frictional losses and losses due to separation. Pope and Rae [10] give an empirical relation for the pressure drop

through a corner with turning vanes.

$$K_t = 0.10 + \frac{4.55}{(\log_{10} Re)^{2.58}} \tag{4.14}$$

4.2 Pressure Loss and Energy Ratios

To determine the pressure loss through the facility, the following procedure was performed. First, the dynamic pressure at the inlet to each section was calculated by using equation 4.15. Next, the total pressure loss across each section, except the fan, was calculated using equation 4.16. The total pressure losses were summed to obtain the HETF's pressure loss. This determined how much pressure would need to be supplied by the fan. This value is seen in tables 4.3, 4.4, and 4.5 as a negative pressure loss, or a pressure rise, across the fan. These tables are the results for a 2x2 core with a velocity of 4000 fpm. The positions are in feet and the pressures are in inches of water. The position, dynamic, total, and static pressures are calculated before each section. The total pressure at each section was obtained by subtracting the pressure loss across the previous section from the previous section's total pressure. The static pressure at each section was then found by using equation 4.17. These results are presented graphically for each core pressure drop case and both testing configurations in figures 4.3, 4.4, 4.5, 4.6, 4.7, and 4.8.

$$Dynamic\,Pressure = P_d = \frac{1}{2}\,\rho U^2 \tag{4.15}$$

$$Total\,Pressure\,Loss = K_t P_t \tag{4.16}$$

$$Static\,Pressure = P_s = P_t - P_d \tag{4.17}$$

Table 4.3: Results using previous data

Pos.	Sec.	K_i	K_{oi}	%	P_d	Loss	P_t	P_s
-9.8	IN 1	0.022	0.007	0.3	0.32	7.1E-3	0.200	-0.12
-5.8	IN 2	0.021	0.021	1.0	1.02	2.1E-2	0.193	-0.82
-1	FAN	0.002	0.002	0.1	1.02	-2.2	0.172	-.84
0	EXP1	0.053	0.069	3.2	1.31	6.9E-2	2.372	1.06
6	ST1	0.003	0.0002	0.0	0.06	1.9E-4	2.203	2.24
7.2	ST2	0.001	0.00008	0.0	0.06	7.9E-5	2.303	2.24
7.7	ST3	6.862	0.429	19.5	0.06	4.3E-1	2.303	2.24
8.2	ST4	0.003	0.0002	0.0	0.06	1.9E-4	1.873	1.81
9.4	C42	0.024	0.001	0.1	0.06	1.5E-3	1.873	1.81
13.4	ST5	0.006	0.006	0.3	1.00	6.0E-3	1.871	0.87
14.6	CORE	0.449	0.449	20.4	1.00	4.5E-1	1.856	0.86
15.6	ST6	0.006	0.006	0.3	1.00	6.0E-3	1.416	0.41
16.8	C21	0.024	0.024	1.1	1.00	2.4E-2	1.410	0.41
18.8	ST7	0.012	0.194	8.8	16.03	2.0E-1	1.386	-14.64
20.2	EXP22	0.054	0.864	39.3	16.03	8.7E-1	1.192	-14.83
22.2	EXP23	0.054	0.054	2.5	1.00	5.4E-2	0.327	-0.68
26.2	ST11	0.013	0.001	0.0	0.06	7.8E-4	0.272	0.21
31.2	ACC	0.003	0.0002	0.0	0.06	1.9E-4	0.272	0.21
32.2	TURN	0.127	0.008	0.4	0.06	7.9E-3	0.271	0.21
36	ST10	0.016	0.001	0.0	0.06	9.7E-4	0.264	.21
42.2	EXIT	1.000	0.063	2.8	0.06	6.3E-2	0.263	0.20
					0.063		0.200	0.137

Table 4.4: Results for the worst case

Pos.	Sec.	K_i	K_{oi}	%	P_d	Loss	P_t	P_s
-9.8	IN 1	0.022	0.007	0.1	0.32	7.1E-3	0.20	-0.12
-5.8	IN 2	0.021	0.021	0.2	1.02	2.1E-3	0.19	-0.82
-1	FAN	0.002	0.002	0.0	1.02	-9.75	0.17	-0.84
0	EXP1	0.053	0.069	0.7	1.31	6.9E-2	9.93	8.62
6	ST1	0.003	0.000	0.0	0.06	1.9E-4	9.86	9.79
7.2	ST2	0.001	0.000	0.0	0.06	7.8E-5	9.86	9.79
7.7	ST3	6.862	0.429	4.4	0.06	4.3E-1	9.86	9.79
8.2	ST4	0.003	0.000	0.0	0.06	1.9E-4	9.43	9.36
9.4	C42	0.024	0.000	0.0	0.06	1.5E-3	9.43	9.36
13.4	ST5	0.006	0.006	0.1	1.00	6.0E-3	9.42	8.42
14.6	CORE	7.990	7.990	82.0	1.00	8.00	9.42	8.42
15.6	ST6	0.006	0.006	0.1	1.00	6.0E-3	1.42	0.42
16.8	C21	0.024	0.024	0.2	1.00	2.4E-2	1.41	0.41
18.8	ST7	0.012	0.194	2.0	16.03	1.9E-1	1.39	-14.64
20.2	EXP22	0.054	0.864	8.9	16.03	8.7E-1	1.19	-14.83
22.2	EXP23	0.054	0.054	0.6	1.00	5.4E-2	0.33	-0.68
26.2	ST11	0.013	0.013	0.0	0.06	7.8E-4	0.27	0.21
31.2	ACC	0.003	0.000	0.0	0.06	1.9E-4	0.27	0.21
32.2	TURN	0.127	0.008	0.1	0.06	7.9E-4	0.27	0.21
36	ST10	0.016	0.001	0.0	0.06	9.7E-4	0.26	0.20
42.2	EXIT	1.000	0.063	0.6	0.06	6.3E-2	0.26	0.20
					0.06		0.20	0.14

Table 4.5: Results for the best case

Pos.	Sec.	K_i	K_{oi}	%	P_d	Loss	P_t	P_s
-9.8	IN1	0.022	0.007	0.4	0.32	7.1E-3	0.20	-0.12
-5.8	IN2	0.021	0.021	1.2	1.02	2.1E-2	0.19	-0.82
-1	FAN	0.002	0.002	0.1	1.02	-1.75	0.17	-0.84
0	EXP1	0.053	0.069	4.0	1.31	6.9E-2	1.92	1.79
6	ST1	0.003	0.000	0.0	0.06	1.9E-4	1.85	1.79
7.2	ST2	0.001	0.000	0.0	0.06	7.8E-5	1.85	1.79
7.7	ST3	6.862	0.429	24.5	0.06	4.3E-1	1.85	1.79
8.2	ST4	0.003	0.000	0.0	0.06	1.9E-4	1.42	1.36
9.4	C42	0.024	0.001	0.1	0.06	1.5E-3	1.42	1.36
13.4	ST5	0.006	0.006	0.3	1.00	6.0E-3	1.42	0.42
14.6	CORE	0.000	0.000	0.0	1.00	0.0	1.42	0.41
15.6	ST6	0.006	0.006	0.3	1.00	6.0E-3	1.42	0.41
16.8	C21	0.024	0.024	1.4	1.00	2.4E-2	1.41	0.41
18.8	ST7	0.012	0.194	11.1	16.03	1.9E-1	1.39	-14.64
20.2	EXP22	0.054	0.864	49.3	16.03	8.7E-1	1.19	-14.83
22.2	EXP23	0.054	0.054	3.1	1.00	5.4E-2	0.33	-0.68
26.2	ST11	0.013	0.001	0.1	0.06	7.8E-4	0.27	0.21
31.2	ACC	0.003	0.000	0.0	0.06	1.9E-4	0.27	0.21
32.2	TURN	0.127	0.008	0.5	0.06	7.9E-4	0.27	0.21
36	ST10	0.016	0.001	0.1	0.06	9.7E-4	0.26	0.20
42.2	EXIT	1.000	0.063	3.6	0.06	6.3E-2	0.26	0.20
					0.06		0.20	0.14

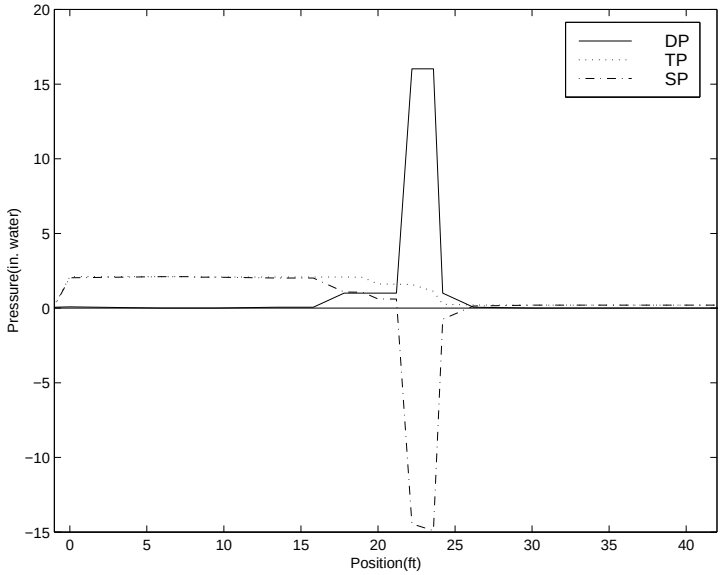

Figure 4.3: Pressures for 1x1 Core at V=4000 fpm (ΔP from data)

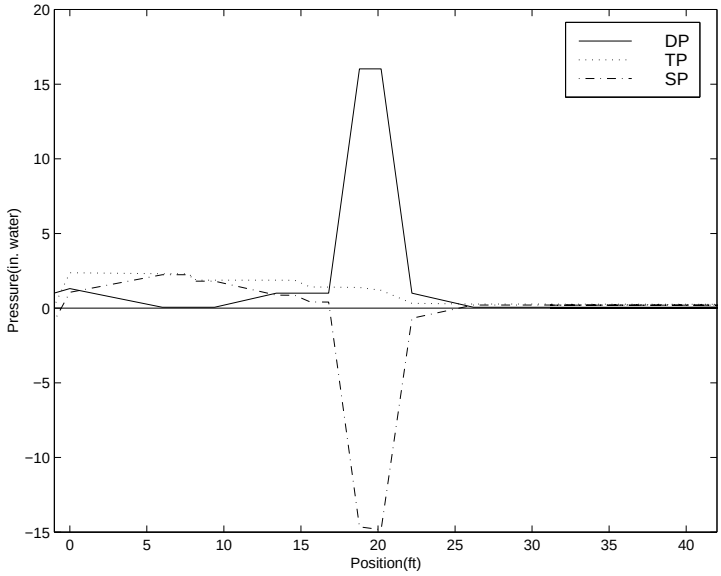

Figure 4.4: Pressures for 2x2 Core at V=4000 fpm (ΔP from data)

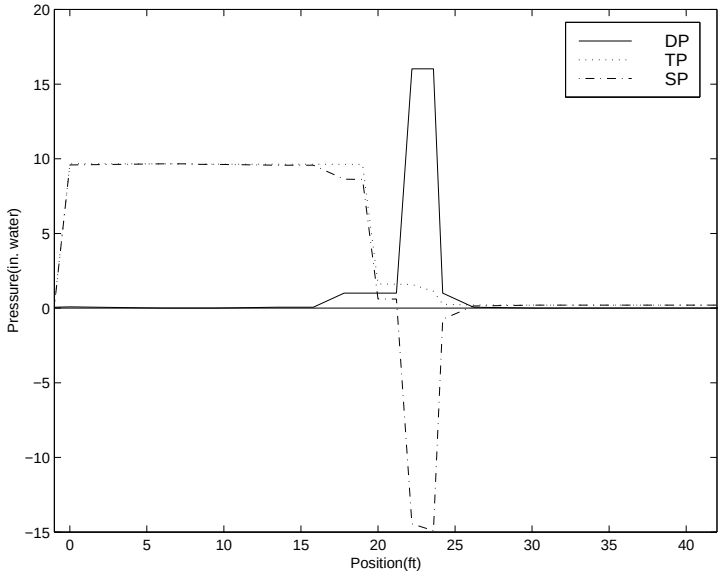

Figure 4.5: Pressures for 1x1 Core at V=4000 fpm (ΔP=8in.)

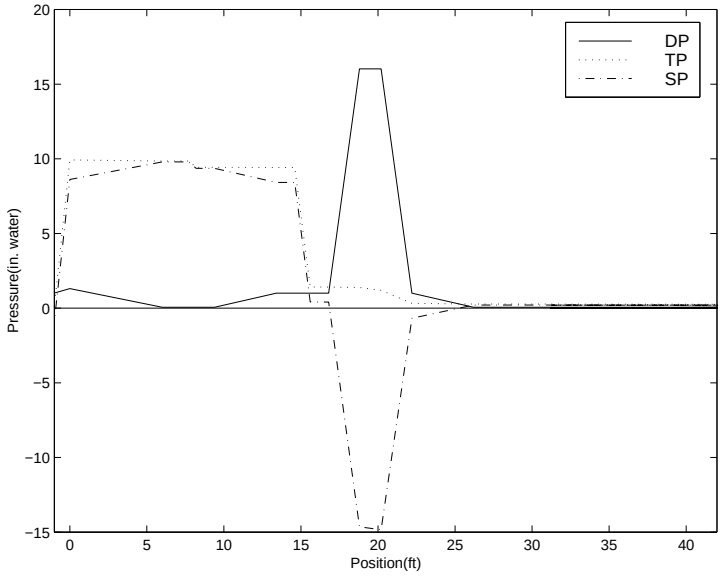

Figure 4.6: Pressures for 2x2 Core at V=4000 fpm (ΔP=8in.)

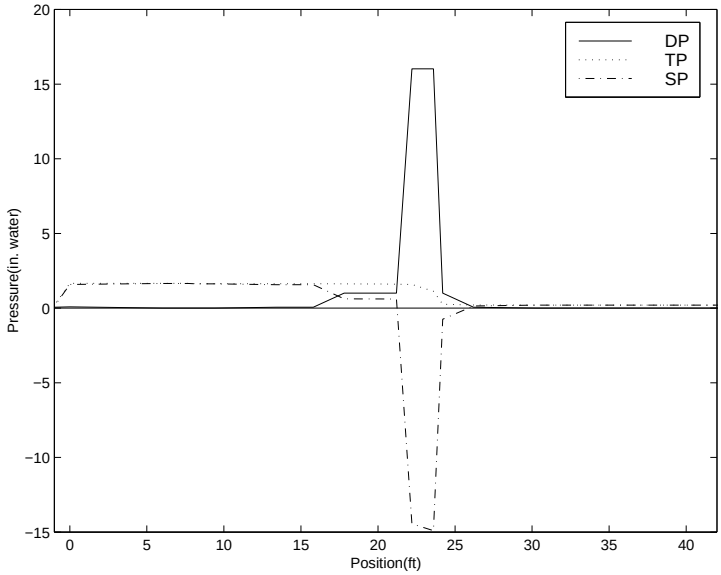

Figure 4.7: Pressures for 1x1 Core at V=4000 fpm (ΔP=0)

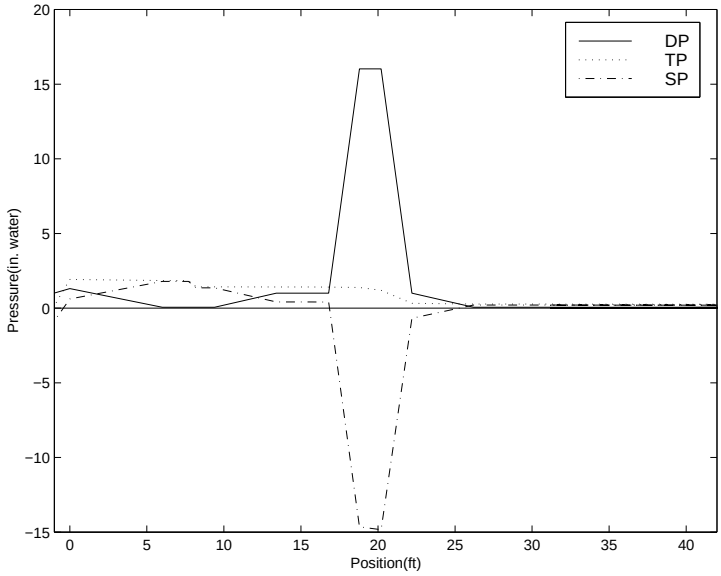

Figure 4.8: Pressures for 2x2 Core at V=4000 fpm (ΔP=0)

The energy loss in a section of the facility is given by [10]

$$\Delta E = K_i \frac{1}{2} \rho A_i V_i^3 \tag{4.18}$$

In order to relate this energy loss to the energy at the test section, a second pressure loss coefficient, K_o, is introduced [13].

$$K_o = K_i \left(\frac{A_o}{A_i} \right)^2 \tag{4.19}$$

where the subscript o refers to the test section and i refers to the individual section.

$$\begin{aligned} \Delta E &= K_i \tfrac{1}{2} \rho A_i V_i^3 \tfrac{A_o V_o V_o^2}{A_o V_o V_o^2} \\ &= K_i \tfrac{1}{2} \rho A_o V_o^3 \tfrac{A_i V_i V_i^2}{A_o V_o V_o^2} \end{aligned}$$

Continuity yields that $A_i V_i = A_o V_o$. Therefore

$$\Delta E = K_i \tfrac{1}{2} \rho A_o V_o^3 \tfrac{V_o^2}{V_i^2}$$

$$\Delta E = K_o \frac{1}{2} \rho A_o V_o^3 \tag{4.20}$$

The energy ratio is defined as [10]

$$ER = \frac{Jet\ Energy}{\sum Circuit\ Losses}$$

Therefore,

$$ER = \frac{\frac{1}{2} \rho A_o V_o^3}{\sum K_o \frac{1}{2} \rho A_o V_o^3} = \frac{1}{\sum K_o} \tag{4.21}$$

Tables 4.6, 4.7, and 4.8 summarize the results for each testing configuration and each pressure loss case at a range of velocities. Figures 4.9, 4.10, and 4.11 show the energy ratio for each pressure loss case and testing configuration as a function of air velocity.

Table 4.6: Pressure Loss and Energy Ratio for Previous Data Case

	2x2 Core		1x1 Core	
Velocity(fpm)	$\Delta P\,(in.\,water)$	ER	$\Delta P\,(in.\,water)$	ER
1000	0.139	0.449	0.121	0.515
2000	0.538	0.465	0.466	0.537
3000	1.210	0.465	1.033	0.545
4000	2.201	0.455	1.913	0.523

Table 4.7: Pressure Loss and Energy Ratio for Worst Case

	2x2 Core		1x1 Core	
Velocity(fpm)	$\Delta P\,(in.\,water)$	ER	$\Delta P\,(in.\,water)$	ER
1000	8.110	0.008	8.092	0.008
2000	8.438	0.030	8.366	0.030
3000	8.985	0.063	8.823	0.064
4000	9.754	0.103	9.466	0.106

Table 4.8: Pressure Loss and Energy Ratio for Best Case

	2x2 Core		1x1 Core	
Velocity(fpm)	$\Delta P\,(in.\,water)$	ER	$\Delta P\,(in.\,water)$	ER
1000	0.109	0.572	0.091	0.684
2000	0.438	0.572	0.366	0.684
3000	0.985	0.572	0.823	0.684
4000	1.751	0.572	1.463	0.684

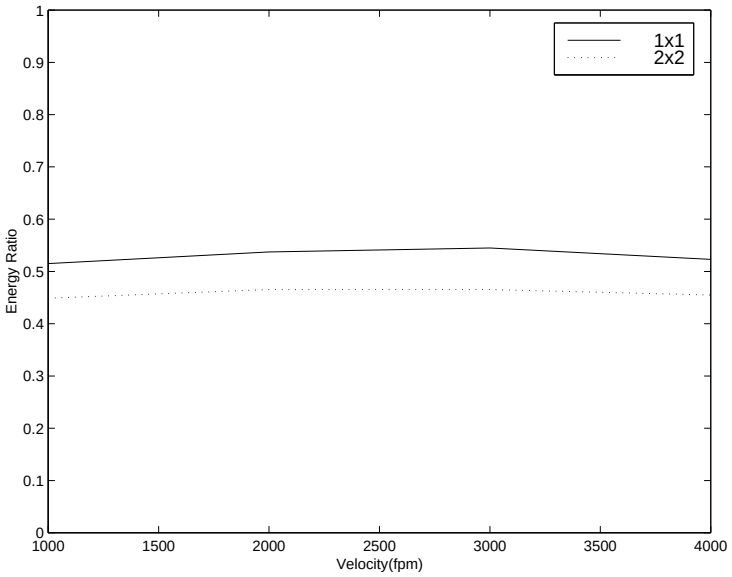

Figure 4.9: Energy Ratio for ΔP from Data

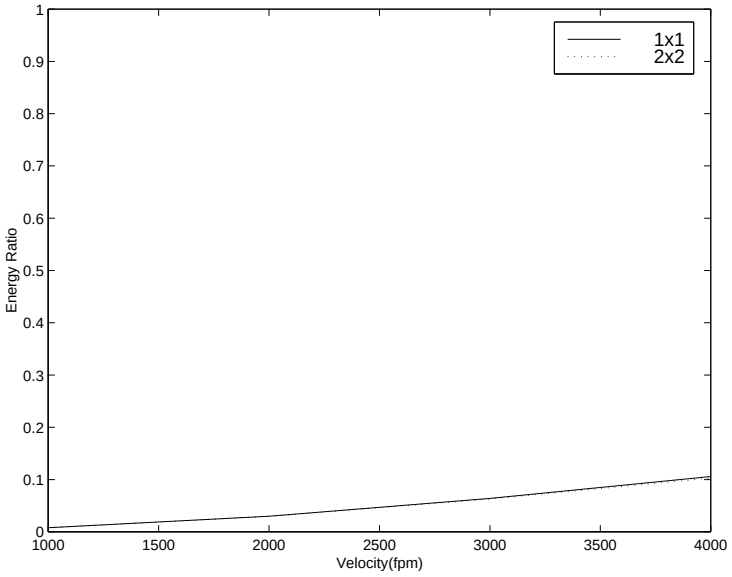

Figure 4.10: Energy Ratio for ΔP=8in

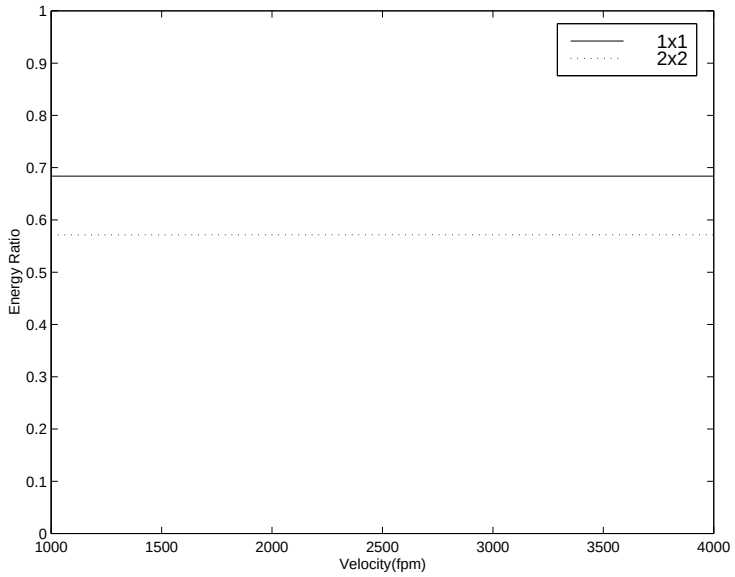

Figure 4.11: Energy Ratio for ΔP=0

It can be seen in table 4.7 and figure 4.6 that the maximum pressure drop through the facility will be 9.75 inches of water. Therefore, a fan that can produce at least 10 inches of static pressure for the entire range of air flows was selected. The pressure that a fan can provide is dependent on the volumetric flowrate of the air. This is illustrated in figure 4.12. This figure shows a static pressure versus flow rate curve for a typical blower. It also has the pressure loss results from tables 4.6, 4.7, and 4.8. When selecting the blower for the facility, it was important to ensure that the tunnel pressure loss curves were inside of the blower performance curve. If this was not the case, the HETF would not be able to operate at all of the desired operating conditions.

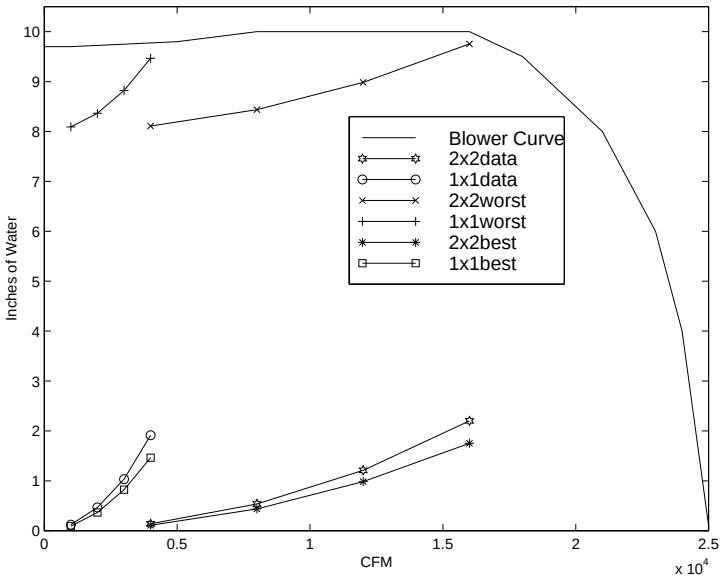

Figure 4.12: Blower Performance Curve and Tunnel Pressure Losses

Chapter 5

Instrumentation

One of the major sources of error associated with the HETF is the instrumentation. Error could result because of incorrect calibration, instrumentation malfunction, or improper installation. Instrumentation was chosen that will lessen the chance of these errors occurring.

5.1 Working Fluid Flow Rate

Several different flow measurement devices are available. Ones that were investigated for possible use with the HETF were turbine meters, pitot-static tubes, and venturi meters.

Turbine meters consist of a turbine that is placed in the flow. The turbine rotates at a rate proportional to the flowrate. This rotation generates an electrical signal that is measured by a voltmeter. A simple bucket and stopwatch calibration will allow the electrical signal to be converted to a flowrate. While turbine meters are easy to install and calibrate, there are some problems associated with them. Throughout the life of the turbine meter, its calibration curve will need to be adjusted. This is because its

components wear over time. The turbine's durability is also a problem. Impurities in the water will interfere with the turbine's components. Eventually, the expensive moving parts need to be replaced.

A pitot-static tube, figure 5.1, measures the difference between the stagnation (total) and static pressures. This difference is the dynamic pressure. Once this pressure is determined, the velocity can by found by

$$V = \sqrt{\frac{2\Delta P}{\rho}}$$

The benefit of a pitot-static tube is that its calibration will not change over time. It is also inexpensive compared to the turbine meter and it is very durable. The problems with a pitot-static tube are that the alignment is critical and there is a possibility of the working fluid leaking where the tube is inserted.

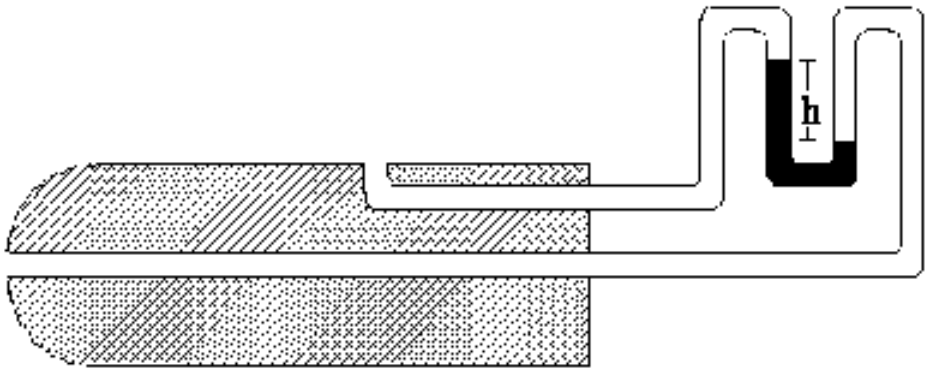

Figure 5.1: Pitot Tube

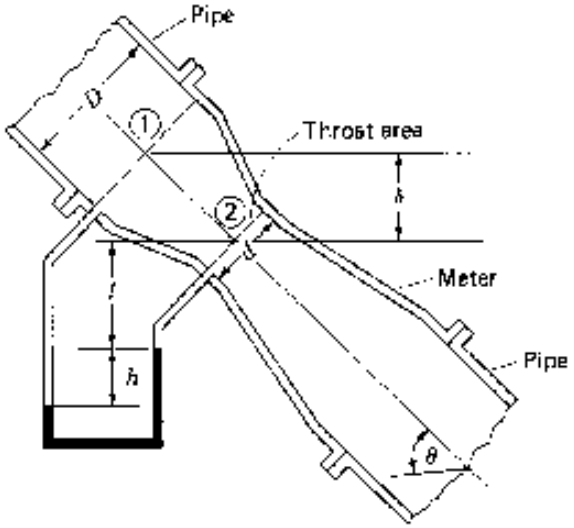

Figure 5.2: Venturi Meter

[18]

A venturi meter, figure 5.2, was selected because it has the advantages of a pitot-static tube and eliminates the disadvantages. A venturi meter is a section of pipe that is inserted into the piping system. The meter has a converging section between the inlet and the throat. It then expands from the throat back to the inlet area. The venturi meters used in the HETF will be horizontal so that potential energy effects can be eliminated. A manometer or pressure transducer measures the pressure difference between the inlet and the throat. This pressure drop is converted to a flowrate by using Bernoulli's equation [18].

$$\frac{p_1}{\rho} + \frac{V_1^2}{2} = \frac{p_2}{\rho} + \frac{V_2^2}{2} \tag{5.1}$$

where point 1 is the inlet and point 2 is the throat. For 1-D flow, continuity yields:

$$\rho V_1 A_1 = \rho V_2 A_2$$

$$V_1 = V_2 \frac{A_2}{A_1} \tag{5.2}$$

Combining equations 5.1 and 5.2

$$\frac{p_1}{\rho} + \frac{V_2^2}{2}\left(\frac{A_2}{A_1}\right)^2 = \frac{p_2}{\rho} + \frac{V_2^2}{2}$$

$$V_2 = \sqrt{\frac{2[(p_1 - p_2)/\rho]}{\left[1 - \left(\frac{A_2}{A_1}\right)^2\right]}}$$

$$q_{theoretical} = V_2 A_2$$

$$q_{theoretical} = A_2 \sqrt{\frac{2\left[(p_1 - p_2)/\rho\right]}{\left[1 - \left(\frac{A_2}{A_1}\right)^2\right]}} \tag{5.3}$$

Since there is friction through the venturi meter, a coefficient of discharge (C_d) is introduced. Shames[18] gives $C_d = 0.995 \pm 1.0\%$ for the conditions that will be seen in the HETF.

$$C_d = \frac{q_{act}}{q_{theoretical}}$$

This leads to equation 5.4 which is used determine the dimensions of the venturi meters.

$$q_{actual} = C_d A_2 \sqrt{\frac{2\left[(p_1 - p_2)/\rho\right]}{\left[1 - \left(\frac{A_2}{A_1}\right)^2\right]}} \tag{5.4}$$

The working fluid will be ranging in flow from 10 - 200 gpm. The pressure transducers that will be used have a range from 0.1 to 1 inch of water.

It was possible to solve equation 5.4 to determine the throat diameter (d_{th}) of the first venturi at 10 gpm with a pressure rise of 0.1 inch of water. This diameter was used to determine the high end flow rate of this venturi with a pressure drop of 1.0 inch. This process was then repeated to find the dimensions of the high flow rate venturi meter. It was then found that two venturi meters would not be able to measure the entire flow range. A third meter was designed to measure the intermediate flow rates. The results can be found in table 5.1.

Table 5.1: Venturi Meter Results

d_{th}(in)	ΔP(in.water)	Flow Rate (gpm)
1.01	0.1 - 1.0	10 - 32
1.42	0.12 - 1.0	25 - 70
1.86	0.1 - 1.0	70 -200

This entire process was repeated using oil as the working fluid. It was found that the slight change in density allowed the venturi meters to operate under approximately the same conditions.

The ASME report on fluid meters [15] gives the appropriate dimensions for venturi meters. The results are summarized in table 5.2.

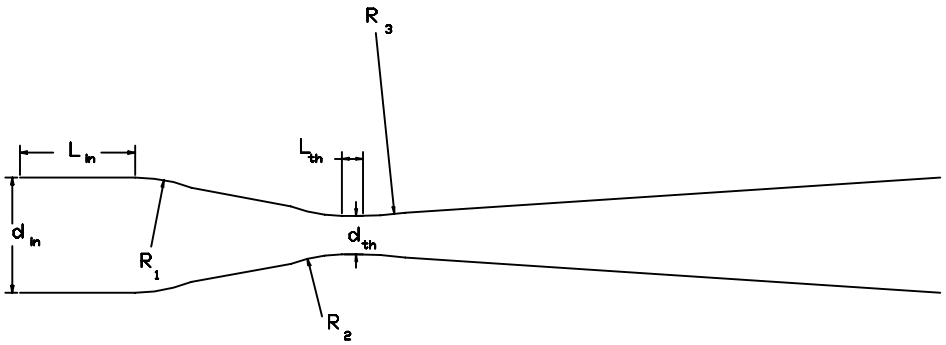

Figure 5.3: ASME dimensions for Venturi Meters

$$L_i \leq d_{in}$$

$$L_t \geq \frac{d_{th}}{3}$$

$$R_1 = 1.375 d_{in}$$

$$R_2 = 3.625 d_{th}$$

$$R_3 = 9.8 d_{th}$$

Table 5.2: Venturi Meter Dimensions (in inches)

Meter	L_{in}	L_{th}	R_1	R_2	R_3
Small	1.01	0.34	4.13	3.67	9.23
Middle	1.42	0.47	4.13	5.16	13.94
Large	1.86	0.62	4.13	6.75	18.26

5.2 Air Flow Rate

It was decided to measure the air flow by using the tunnel as a venturi meter. Four static pressure taps (one on each side of the HETF) will be installed upstream and downstream of the contraction after the test section which will measure the pressure drop across the change in areas. Equation 5.4 gives the flow rate as a function of the pressure drop. If the pressure was measured at a section with the same area as the test section, the pressure drop will be in the thousandths of inches of water for the low range of velocities. It is very difficult to measure this little of a pressure drop. In order to increase the pressure drop, the HETF is contracted to a section 4 times smaller in area than the test section. This will increase the pressure drop to tenths of inches of water for the lower velocities.

5.3 Temperature measurement

Temperature sensors that were investigated were resistance temperature detectors (RTD) and thermocouples. An RTD is a wound wire device [20]. The wire resistance increases as the temperature increases. This change in resistance is measured and converted to a temperature. Thermocouples are made by joining two dissimilar metals. The junction of these metals create a voltage that is dependent on the temperature. The voltage is read and converted to a temperature. While RTDs are more accurate,

their cost is much more than a thermocouple. One thousand feet of thermocouple wire costs around $500. An RTD can cost as much as $100. Since many sensors will be needed, it was decided to use thermocouples.

The inlet air temperature is assumed to be uniform across the facility's cross section. Therefore, the inlet air will be measured by a single thermocouple. The outlet air temperature cannot be assumed to be uniform. The exit air will be measured by an array of 25 thermocouples mounted in five $\frac{1}{4}$ inch diameter cylinders, figure 5.4. The thermocouple's readings will be averaged together to obtain the exit air temperature. The water temperature will also be measured using thermocouples. Three

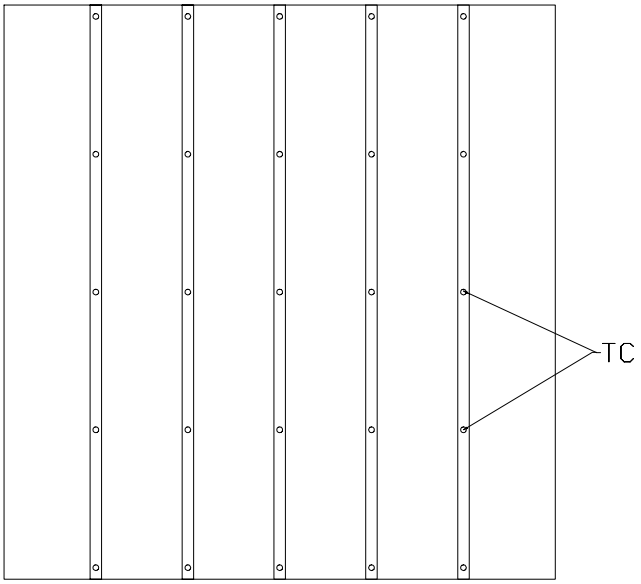

Figure 5.4: Thermocouple Arrangement

thermocouples will be inserting into the piping before and after the heat exchanger and their readings will be averaged together.

5.4 Data Acquisition

The signals produced by the thermocouples and pressure transducers will be read by an analog/digital (A/D) board. Since the thermocouple's signal is on the order of microvolts, signal conditioning will need to amplify this voltage to make it readable. A/D boards can be obtained which perform this conditioning. The A/D board will be connected to an IBM PC clone. This computer will read the data obtained by the A/D board and analyze it. Many different data acquisition software packages are available. The TRL's HETF uses Labview software. This software is relatively easy to learn and operate. The software will use equation 1.4 to determine if the system is operating properly while the data is being obtained. This allows the user to identify any problems with the data acquisition before the test is completed. This will save much time in the testing process. The data will be saved to a data file which can be inputted into the customer's visual basic program to determine the Colburn and friction factors for the heat exchanger. This program takes into account the number of air and water passages, the dimensions of the core, and the number and configuration of the fins. The pumps and blower have a motor controller that has a computer interface which allows the user to control the working fluid and air flowrates from the computer. This will make testing quicker and easier.

Chapter 6

Cost and Additional Considerations

The majority of the design of the HETF has been finished. Drawings of each component of the facility have been completed and are ready to be submitted for manufacturing. There are some items that need to be addressed before the facility can be constructed and operated. This chapter discusses the cost of the HETF, the remaining work, and acoustical considerations.

6.1 Cost of the HETF

The approximate cost of the HETF has been determined. Several different manufactures of pumps, boilers, and blowers were contacted to provide quotes on the components. Ones were selected that best fit the criteria presented in this report. The cost of the facility components can be seen in tables 6.1 and 6.2. The labor costs for each component are rough estimates. These costs were approximated with the aid of the machinists from Engineering Design Services at the University at Buffalo.

Table 6.1: Cost of the HETF

Component	Description	Cost
Boiler	750,000 BTU/hr	$13,608
Pumps(2)	200 GPM 25psi	10,390
Blower	10,000 CFM 10" water	7,100
Ducting/Framing	see table 6.2	23,998
Electrical	wiring, etc.	500
Instrumentation		
Venturi meters(6)		3,480
Pressure Transducers(3)	for working fluid	1,560
Thermocouples(32)		896
Pressure Transducers(2)	for air flow	720
Computer/Data Acquisition		
IBM PC Clone		2,000
Computer Boards		1,056
Lab View Software		750
Instrumentation Panels		1,000
TOTAL		**67,058**

6.2 Pending Decisions

Before the HETF can be constructed, the centerline height of the facility must be decided upon. This is dependent on the manner in which the blower is supported. Once this is decided, the lengths of the supporting legs can be determined.

Modifications to the location where the HETF will be operated in are necessary. Openings in the wall for the inlet and outlet of the facility will need to be made. These holes will be covered with a screened enclosure to prevent contaminants from entering the HETF. It is also necessary to supply electricity to power the major components of the HETF.

Table 6.2: Cost of the Ducting/Framing

Section	**Labor**	**Materials**	**Total**
Inlet	$1,500	$ 88.00	$1,588.00
1st Expansion	1,000	229.37	1,229.37
1st Straight	250	66.94	316.94
2nd Straight	250	59.74	309.74
3rd Straight	250	59.74	309.74
4th Straight	250	66.94	316.94
1st Contraction	1,000	108.11	1,108.11
5th Straight	500	40.43	540.43
6th Straight	500	72.73	572.73
2nd Contraction	750	39.34	789.34
7th Straight	250	26.63	276.63
8th Straight	250	41.04	291.04
3rd Contraction	500	17.38	517.38
9th Straight	250	29.51	279.51
2nd Expansion(1)	250	34.02	284.02
2nd Expansion(2)	500	75.28	575.28
2nd Expansion(3)	1,000	211.26	1,211.26
Adjustable Section	750	73.33	823.33
Turn	1,500	196.39	1,696.39
10th Straight	500	149.55	649.55
11th Straight	500	154.41	654.41
Return	1,500	275.00	1,775.00
Pluming	1,000	4271.50	5,271.50
TOTAL (10% has been added to materials for waste)	**15,000**	**8998.48**	**23,998.48**

6.3 Acoustical Considerations

In order for the HETF to operate under desirable conditions, it is important to limit the noise produced by the facility. A major source of noise is generated by the pumps and blower. This noise is preventable to some degree by the proper selection of components. Noise could also be generated by the flow of air through the facility. This source is difficult to predict but it can be remedied if it occurs.

6.3.1 Pump and Blower Noise

Sound is measured by determining the change in air pressure caused by the sound wave. The sound pressure level (SPL) is measured in decibels (dB) and defined by [2]

$$SPL = 20log_{10}\frac{p}{0.0002} \tag{6.1}$$

where p is the rms sound pressure in μbar. The sound pressure is compared against a reference value of 0.0002μbar. This value was selected because it represents the average threshold of hearing for a human [2]. Therefore, a sound pressure of 0.0002 μbar would have a sound pressure level of 0 dB. The SPL of several common sounds is listed in table 6.3 [6].

Table 6.3: Some Sound Levels (dB)

Threshold of hearing	0
Rustle of leaves	10
Whisper (at 1m)	20
City street, no traffic	30
Office, classroom	50
Normal conversation (at 1m)	60
Rock group	110
Threshold of pain	120
Jet engine (at 50m)	130
Saturn rocket (at 50m)	200

It is impossible to design pumps and blowers that will not produce noise. The manufactures design these components to be as quiet as possible. To limit the noise generated by the HETF, pumps and a blower were selected that have a SPL of under 85 dB for all operating conditions. This sound level is accepted as a tolerable level of noise.

6.3.2 Noise Generated by Airflow

Noise can also be generated by the flow of air through the HETF. One source of this sound is vortex shedding. Vortices are created and shed when the boundary layer separates. While great care has been taken to prevent separation in the HETF, it still could occur as a result of the expansions, turning section, thermocouple probes, and the heat exchanger being tested. It is very difficult to predict if noise will be generated by the shed vortices. However, if unacceptable is noise generated by the HETF, then the source of this sound will need to be identified. Standard methodology for sound and vibration analysis exists and will have to be employed. Techniques that can be used to determine the source of the noise can be found in the discussions and references in [1] and [7].

Once the source is identified, the noise can be eliminated several ways. If the sound is airflow speed dependent, the easiest way may be to not operate the facility at that air speed. This could move the frequency out of the acoustic range. If the sound persists, a redesign of the source component might be necessary. If it is not possible to change the configuration of the source, an acoustic damper could be placed at the source to absorb the sound waves. One of these methods should eliminate the source of noise.

Chapter 7

Summary

All of the major design issues presented in the introduction have been satisfied. A facility that can use both water and oil as working fluids has been designed. The range of air and working fluid flow rates and the ability to vary the inlet air temperature leads to a wide range of operating conditions. The configuration of the HETF can be easily changed to accommodate different sizes of heat exchangers. This facility is very versatile and can be used to successfully test the performance of heat exchangers.

There is one benefit of the HETF that has not yet been discussed. During the heating season, the heated air leaving the facility can exit into the room where it is located. This will decrease the cost of heating the building which will offset some of the operating cost associated with the facility.

This report concerned the design of a particular HETF. The available space for the HETF, the types of heat exchangers being tested, and the configuration of the room where it will be housed have all been taken into consideration. These factors determined the geometry of the HETF. Keeping these geometric constraints in mind, techniques were used to determine the proper design of the contractions, expansions,

and turning section. It was also shown how the boiler, pumps, and blower were selected for the facility.

Although this design was for a specific HETF, the information presented herein can be used to design any HETF. A designer can use the techniques to determine the correct blower, pumps, and boiler. Correlations have been presented which can be used to design the expansions, turning sections, and contractions for any facility. This report can therefore serve as a HETF design handbook.

Appendix A

CFD Diffuser Analysis

A CFD study was performed to assist in the diffuser design. A code that was previously developed at the University at Buffalo was used. This code solves the Navier-Stokes equations in two dimensions using the finite volume method with staggered grids. This code can be used to determine the behavior of an axisymmetric diffuser. While the diffusers used in the facility are rectangular and not conical, the results obtained from the code can be compared to Kline's [11] results for conical diffusers. This will help to confirm the correlations used in chapter 4.

Curvilinear grids were used to represent the geometry of the diffuser. The grid was made using an algebraic grid generator which included stretching in the radial direction. Stretching was used so that more grid points will be located towards the wall. This will increase the resolution in the boundary layer. An example of the grid can be seen in figure A.1. The darkening towards the wall is a result of the grid stretching. The grid used in the program had 80 points along the diffuser and 200 points in the radial direction. The grid included a straight section before the diffuser to represent the actual diffuser configuration in the HETF.

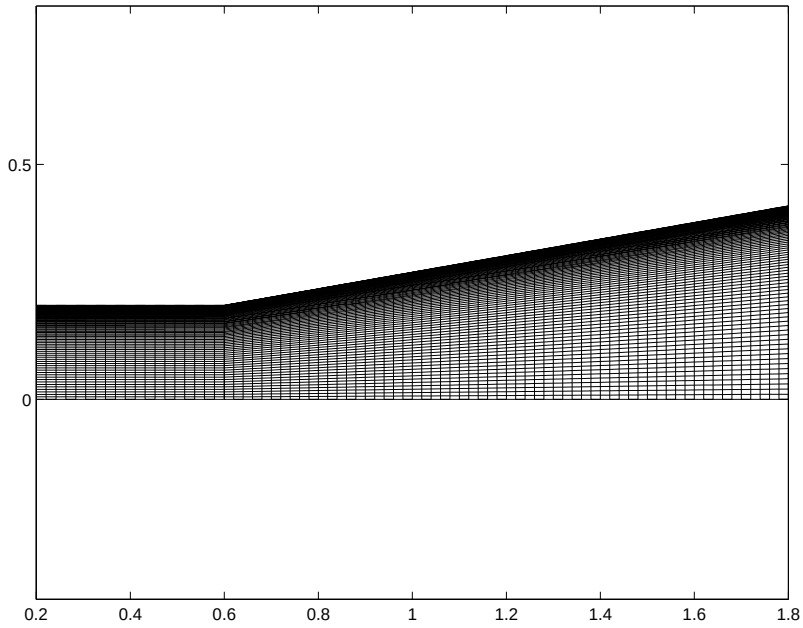

Figure A.1: Grid used in CFD program

It was necessary to provide the code with an inlet velocity. A uniform inlet condition was first used. It was found that the coefficient of pressure recovery was greater than the ideal coefficient of pressure recovery for some angles, which is not physically possible. Since these results were invalid, a non-uniform inlet velocity distribution was then used. Schlichting [17] presents results which determine that the velocity profile for turbulent flow in pipes is given by

$$u\left(y\right) = U\left(\frac{R-y}{R}\right)^{\frac{1}{n}} \tag{A.1}$$

where U is the centerline velocity, R is the radius of the pipe, y is the distance from the centerline, and n is an exponent dependent on the Reynolds number. For the range of Reynolds numbers that will occur in the facility, n=7. This inlet profile is a more realistic condition and it did yield much better results.

In order to compare the results to Kline's tests, it was important to perform the simulations under conditions similar to them. It was also desired to obtain results for conditions similar to ones that will be used in the HETF. The centerline velocity, U, was 50 f/s, which is typical of speeds that will be used in the facility. The length to width ratio, L/D, of the diffuser was 6.0. The Reynolds number based on the inlet diffuser diameter was 133,000.

The program solved for the velocity and static pressure at each point. Using the results along with equation 4.8, it was possible to determine the relationship between the coefficient of pressure recovery, C_{pr}, and the total divergence angle, 2θ. These results are presented in figure A.2 along with data obtained from Kline's results [11], figure 4.2.

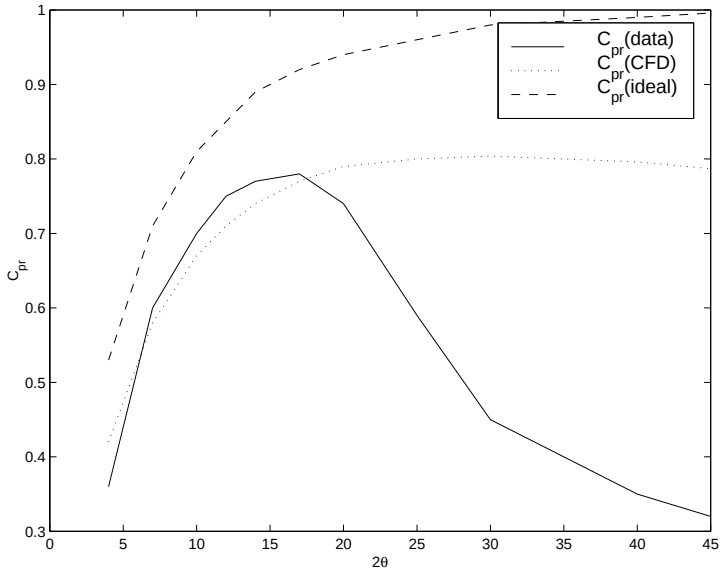

Figure A.2: C_{pr} from data and CFD

Figure A.2 shows that the results predicted by the CFD code agree with Kline's data up to 2θ=15°. It can be seen in figure 2.4 that this point falls on the line of appreciable stall. There are several reasons why the code doesn't agree with diffuser data for large angles. The first is that the code solves for laminar flow. The flow through the diffuser is clearly turbulent. The code can predict laminar separation, but turbulent separation behaves differently. Once appreciable stall begins to occur, the results will be invalid. Another problem is that the code solves for a steady flow. The diffuser lies in the large transitory stall regime for the larger angles. In this regime, the flow fluctuates with time and stall regions are formed and swept out of the diffuser. A steady state program will not be able to obtain reliable results in this regime. Another limitation is the boundary layer resolution. Although there is stretching in the grid which places more points towards the wall, there still isn't enough points to obtain accurate results in the boundary layer. Increasing the number of points would have been possible, but this would increase the time needed for the program to reach a solution. Because of the other limitations with the code, it was decided that more resolution would not have been beneficial.

Since the code's results agree with results obtained from testing for smaller angles, the CFD results can be used to predict diffuser performance in this regime. A major consideration with the diffusers was to maintain a uniform flow for testing. Figures A.3, A.4, and A.5 show the velocity distribution at the inlet, middle, and the outlet of the diffuser. It can be seen in these figures that the velocity is becoming more uniform along the length of the diffuser.

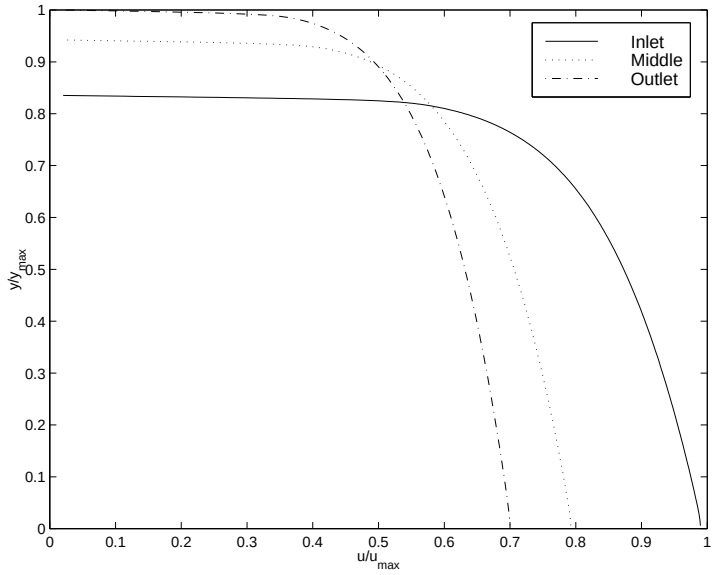

Figure A.3: Velocity Distribution for 2θ=4

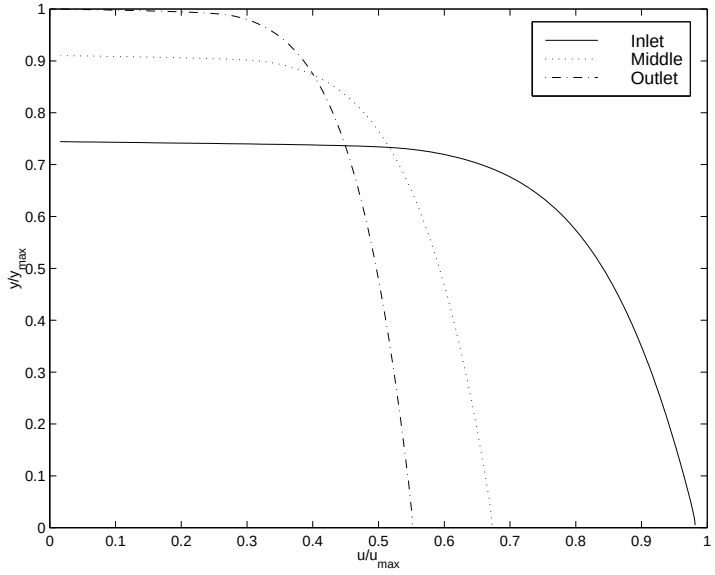

Figure A.4: Velocity Distribution for 2θ=7

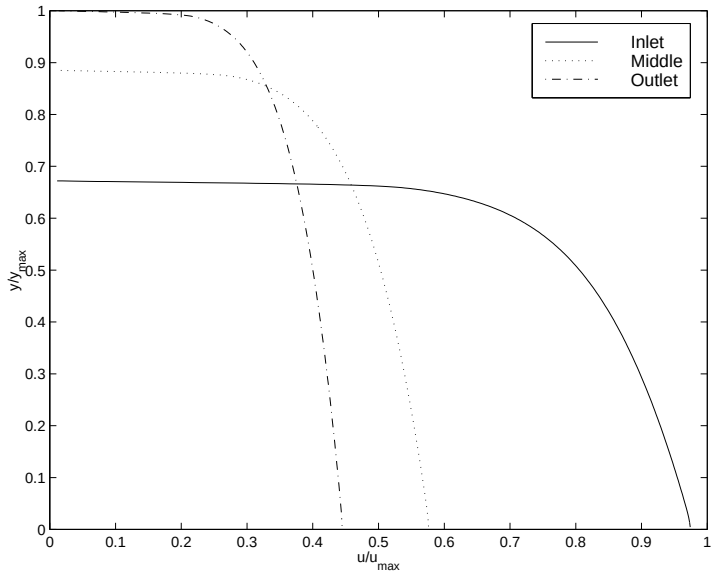

Figure A.5: Velocity Distribution for 2θ=10

Although the code has limitations, it did reinforce the correlations used to design the diffusers. To minimize the total pressure loss through the diffusers, it is necessary to have small divergence angles. If the diffuser was designed without the splitter plates, an unsteady and non-uniform flow would occur and there would be an unacceptable pressure loss.

Bibliography

[1] Robert C. Chanaud. Basic mechanisms of noise generation by fluids. In *Noise and Fluids Engineering*, 1977.

[2] Ernest O. Doebelin. *Measurement Systems Application and Design.* McGraw Hill, 1990.

[3] Fuh-Min Fang. A design method for contractions with square end sections. *Transactions of the ASME - Vol. 119*, pages 454–458, June 1997.

[4] William K. George, 1997. University at Buffalo, Personnal communication.

[5] S.M. Gorlin and I.I. Slezinger. *Wind Tunnels and Their Instrumentation.* S. Monson, 1964.

[6] David Halliday, Robert Resnick, and Jearl Walker. *Fundamentals of Physics.* John Wiley & Sons, 1993.

[7] Jay C. Hardin. Noise calculation on the basis of vortex flow models. In *Noise and Fluids Engineering*, 1977.

[8] Frank P. Incropera and David P. De Witt. *Introduction to Heat Transfer.* John Wiley and Sons, 1990.

[9] Peter W. Runstadler Jr., Francis X. Dolan, and Robert C. Dean Jr. *Diffuser Data Book.* Creare Inc., 1975.

[10] William H. Rae Jr. and Alan Pope. *Low Speed Wind Tunnel Design.* John Wiley and Sons, 1984.

[11] S.J. Kline, D.E. Abbott, and R.W. Fox. Optimum design of straight-walled diffusers. *Journal of Basic Engineering*, pages 321–331, Sept., 1959.

[12] Stephen J. Kline. On the nature of stall. *Journal of Basic Engineering*, pages 305–320, Sept., 1959.

[13] R.D. Marshall. Performance requirements and preliminary design of a boundary layer wind tunnel facility. Technical Report NSBIR 85-3168, U.S. Department of Commerce, National Bureau of Standards, 1985.

[14] Katsuhiko Ogata. *Modern Control Engineering.* Prentice-Hall Inc., 1970.

[15] ASME Research Committee on Fluid Meters. *Fluid Meters; Their Theory and Application.* ASME, 1971.

[16] L.R. Reneau, J.P. Johnston, and S. J. Kline. Performance and design of straight, two-dimensional diffusers. *Journal of Basic Engineering*, pages 141–150, March, 1967.

[17] H. Schlichting. *Boundary-Layer Theory.* McGraw-Hill, 7th edition, 1979.

[18] Irving H. Shames. *Mechanics of Fluids.* McGraw Hill Inc., 1992.

[19] Jimmy Tan-Atichat. *Effects of Axisymmetric Contractions on Turbulence of Various Scales.* PhD thesis, Illinois Institute of Technology, 1980.

[20] Watlow, Inc. *Heaters, Sensors, and Controls.*